Revisiting reverse osmosis as a mechanism contributing to metal zoning in porphyry copper deposits

M.S. Japas [a,*], N.A. Rubinstein [a], A.L.R. Gómez [a,b]

[a] *CONICET-Universidad de Buenos Aires. Instituto de Geociencias Básicas, Aplicadas y Ambientales - CONICET (IGeBA). Buenos Aires, Argentina*
[b] *Universidad de Buenos Aires, Facultad de Ciencias Exactas y Naturales, Departamento de Ciencias Geológicas, Buenos Aires, Argentina*

ARTICLE INFO

ABSTRACT

The Mid Permian San Pedro porphyry deposit in the San Rafael Massif (central-western Argentina) offers a valuable opportunity to contribute in the understanding of ore concentration mechanisms operating during the phyllic alteration stage. In this deposit, two generations of low-temperature D-veins (D_1 and D_2) formed during the phyllic alteration stage. The D_2-type veins show an atypical Cu-Ag sulfide paragenesis consisting mainly of galena, chalcocite, native silver, chalcopyrite and bornite, which can not be explained using the traditional cooling model. Based on previous research and own data, we test Reverse Osmosis as a possible mechanism contributing to D_2-vein ore deposition. Reverse Osmosis is a pressure-driven retention-selective membrane filtration process resulting in solute/ion retention on the high-pressure side of the membrane.

D_2-veins from San Pedro porphyry formed at 211°–176 °C during transient fluid overpressures produced by the hydrothermal sealing that followed the earlier D_1-vein formation. Besides the temperature range and the declining orogeny, physico-chemical conditions were optimal for Reverse Osmosis to activate because the presence of a semi-permeable phyllic membrane and a transmembrane pressure gradient with hydrothermal fluid pressure exceeding the relatively low stress normal to the fracture walls (σ_n). This particular condition activated Reverse Osmosis, allowing to get similar membrane rejection values for Cu and Ag chloride complexes at lower fluid temperatures, causing the decrease of the osmotic differentiation performance, and the consequent coeval precipitation of Cu and Ag sulfide minerals.

1. Introduction

Porphyry copper deposits, which represent the world's largest source of Cu, consist of large volumes of host rocks ($10->100$ km³) affected by hydrothermal alteration with disseminated and in-vein mineralization centered on Cu-bearing porphyry stocks.

Several papers provide a comprehensive review of the main features of porphyry copper deposits (*e.g.,* Hedenquist and Richards, 1998; Tosdal and Richards, 2001; Cooke et al., 2005; Seedorff et al., 2005; Sillitoe, 2010; Tosdal and Dilles, 2020; Dilles and John, 2020; among others). These deposits occur in subduction-related scenarios (including magmatic-arc, flat-slab subduction and post-collisional settings) where the action of the hydrothermal fluids results in alteration-mineralization patterns on the surrounding rocks with the alteration patterns displaying a broad-scale zoning that comprises, centrally from the bottom upward, potassic, phyllic, advanced argillic and propylitic alteration halos. General metal zoning (Fig. 1) comprises a Cu ± Mo zone (usually linked to the potassic alteration stage) centered on the porphyry stock roughly surrounded by a base-metal zone (Pb-Zn-Ag, usually linked to the phyllic alteration stage) with metal zoning reflecting changes in fluid compositions, as well as metal transport and precipitation mechanisms.

It is well known that multiple and competing physico-chemical factors control porphyry copper deposit formation (Hedenquist and Richards, 1998; Tosdal and Richards, 2001; Cooke et al., 2005; Seedorff et al., 2005; Sillitoe, 2010; Kouzmanov and Pokrovski, 2012; among many others). Although porphyry copper deposits have been intensively studied because they are a major source of Cu, some aspects of their genesis still remain unclear, such as the metal zoning controls. Traditionally, metal zoning was described to be largely controlled by temperature assisted by chemical fluid-rock interaction (*e.g.,* Ulrich and Heinrich, 2001; Landtwing et al., 2005; Rusk et al., 2008). However, these controls cannot explain metal depletion *vs.* metal enrichment during chlorite-sericite and sericite (phyllic) overprints, or why Zn can concentrate in polymetallic veins and/or overprinting the Cu-enriched

potassic cores (see Sillitoe, 2010); nor why the sulfur isotope zoning observed in some alkalic porphyry deposits does not match with the cooling model for sulfide deposition (Deyell, 2005). More recently Japas et al. (2015) propose Reverse Osmosis (RO, a pressure-sensitive membrane filtration process involving retention of solutes at the metal ionic and metal complex ranges of ~ 2–15 Å) as a mechanism contributing to metal zoning, complementary to cooling and chemical fluid neutralization due to water–rock interaction. These authors argue that, in presence of a semi-permeable phyllic (clay) membrane, differences in the relative rejection values for metal ions (and metal complexes) at the temperature ranges of the phyllic alteration stage, could lead to the metal zoning observed in the El Infiernillo porphyry copper deposit (Argentina) which could not be fully explained through the cooling and chemical fluid-rock interaction. According to Japas et al. (2015), RO is a viable self-generated mechanism, compatible with the presence of natural potential-energy gradients and also with the geological time rates linked to porphyry copper deposit formation, since it is a slow and low-energy consumption process.

In this contribution we use the RO theoretical background described in Japas et al. (2015) to elucidate the origin of the atypical ore paragenesis of a vein system (*La Salvadora* vein) linked to the low temperature phyllic stage of the Permian San Pedro porphyry copper deposit, with the aim of testing the validity of the proposed RO mechanism in controlling ore metal distribution in porphyry systems.

2. Geology of the San Pedro area

The San Pedro porphyry copper deposit is located in the San Rafael Massif, Argentina (Fig. 2a), which is characterized by widespread volcanic and pyroclastic rocks of Gondwanan (Late Paleozoic - Early Mesozoic) age, known as the Choiyoi Magmatic Cycle, which comprises a lower and upper section (Llambías et al., 1993; Kleiman and Japas, 2009; see Table 1). The Early Permian lower Choiyoi section was emplaced under a transpressional regime (the San Rafael Orogeny) and consists of medium to high K andesites, dacites and low SiO_2 rhyolites with geochemical characteristics typical of continental arc magmatism (Kleiman and Japas, 2009; Gómez et al., 2015; and references therein). The Late Permian upper Choiyoi section was emplaced under a transtensional regime (the Post-San Rafael extension) and consists of high K,

high SiO_2 rhyolites, dacites and andesites with geochemical characteristics transitional between subduction and continental intraplate settings (Llambías et al., 1993; Kleiman and Japas, 2009; Gómez et al., 2015; and references therein). Two stages of deformation within the San Rafael orogeny were recognized (Japas and Kleiman, 2004; Kleiman and Japas, 2009). The first stage of dextral N–NNW transpression took place before the onset of the lower Choiyoi section, and was followed by the second stage of sinistral WNW transpression that was coeval with the emplacement of the Lower Choiyoi as well as the basal unit of the upper Choiyoi section (Table 1).

2.1. The San Pedro porphyry copper deposit

The San Pedro porphyry copper deposit is hosted and genetically linked to the lower Choiyoi section that, in the deposit area, consists of pyroclastic andesitic breccias and dacitic tuffs intruded by a subvolcanic intrusive of intermediate composition named San Pedro Porphyry and andesitic dykes (Gómez et al., 2015). The pyroclastic andesitic breccias consist of andesitic clasts in a very fine-grained andesitic matrix. The dacitic tuffs are composed of quartz, feldspar, and mica crystaloclasts, volcanic lithic fragments, and recrystallized shards and *fiamme* in a felsic matrix. The San Pedro Porphyry (Fig. 2b) consists mainly of a pre-mineralization dioritic-tonalitic facies of Permian age (263.1 ± 4.2 Ma) with a porphyritic to granular texture composed of plagioclase, minor clinopyroxene, scarce biotite, magnetite, and a quartz and K-feldspar interstitial intergrowth. At the southeast margin of the San Pedro Porphyry, scarce outcrops of a syn-mineralization dacitic facies, composed of plagioclase, biotite, quartz, and amphibole phenocrysts in a very fine-grained groundmass, have been recognized. The relationship between both facies is unclear (Gómez et al., 2015). Post-mineralization andesitic dykes composed of plagioclase, amphibole, and scarce K-feldspar phenocrysts and a fine-grained plagioclase and quartz groundmass intruded the pyroclastic breccias, the dacitic tuffs and the San Pedro Porphyry. Kinematics and structural control at the San Pedro porphyry copper deposit reveal the change in the tectonic regime from transpressional to transtensional during its formation, confirming that it formed during the declination of the San Rafael Orogeny (Japas et al., 2021).

Hydrothermal alteration affects the San Pedro Porphyry and the surrounding pyroclastic rocks (Fig. 2b). Three alteration stages were
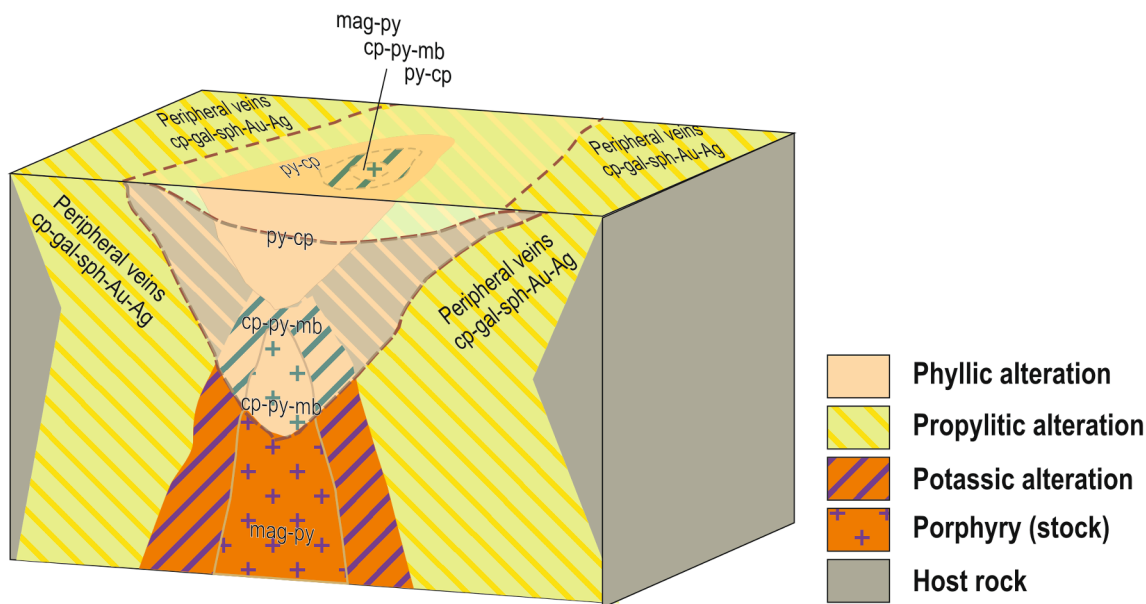

Fig. 1. Anatomy of a porphyry-type deposit. Simplified block diagram showing the distribution of alteration zones and metal zoning (modified from Sillitoe, 2010). Telescoping (the overprinting of the different alteration zones) is also represented. mag: magnetite; py: pyrite; cp: chalcopyrite; mb: molybdenite; gal: galena; sph: sphalerite.
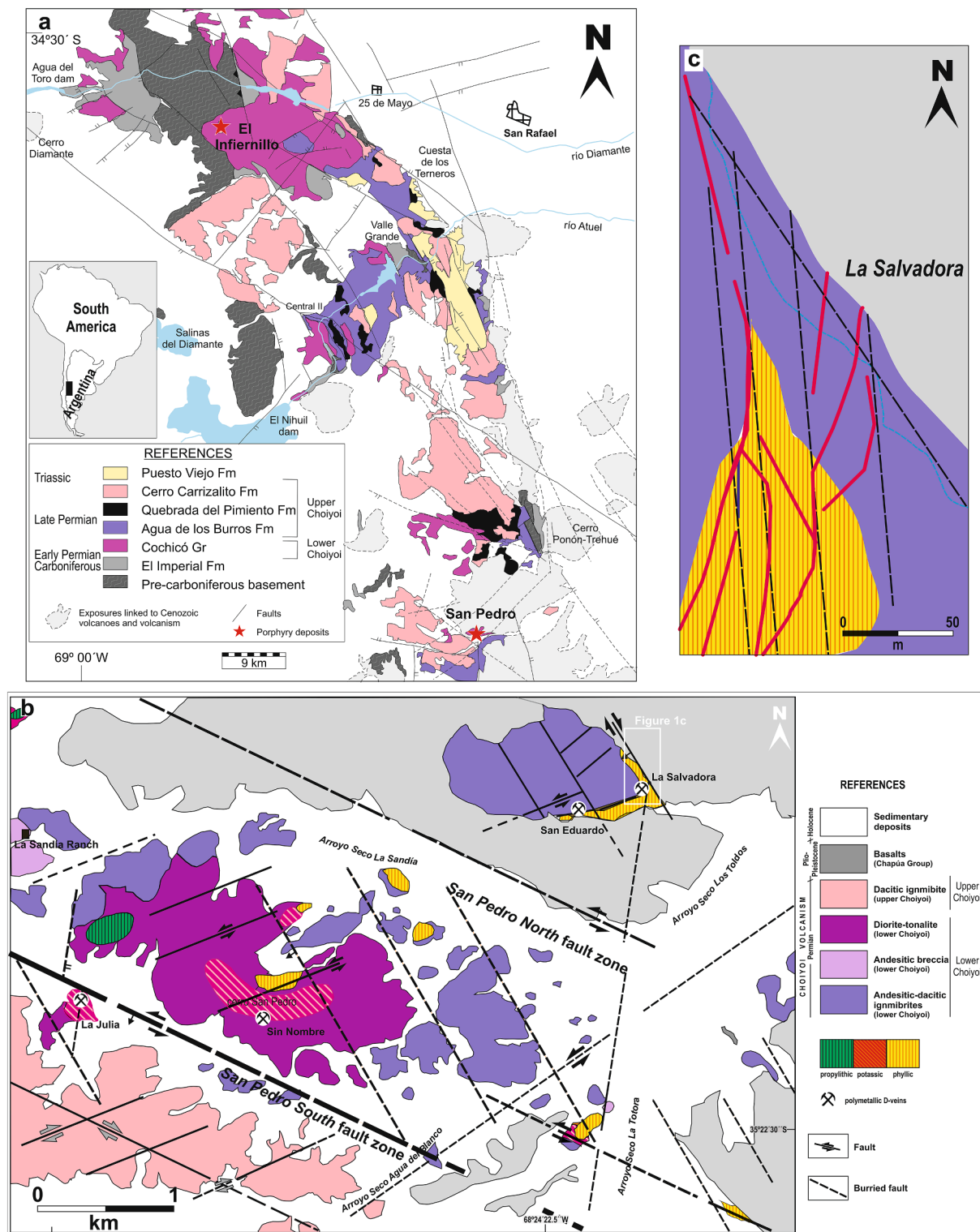
Fig. 2. The San Pedro porphyry-type deposit. a. Geological map of the San Rafael Massif (after Kleiman and Japas, 2009). **b.** Geological map of the San Pedro porphyry deposit (modified from Gómez et al. 2015 and from Japas et al., 2021). **c.** Geological map of the *La Salvadora* D₂-vein area (after Davicino, 2008).

described in Gómez et al. (2021). The early alteration stage comprises pervasive propylitic and potassic alteration. The propylitic alteration occurs as replacement in the western part of the San Pedro Porphyry (Fig. 2b), and consists of chlorite, epidote, carbonate and tremolite-actinolite with minor titanite, albite, prehnite and magnetite. Chlorite-epidote veinlets are locally observed. The early potassic alteration is mainly developed in the central part of the San Pedro Porphyry (Fig. 2b)

and consists of pervasive K-feldspar and quartz with minor tremolite-actinolite and albite assemblage, and barren quartz-K-feldspar veinlets. The main alteration stage is defined by potassic alteration and includes an early K-feldspar alteration with associated Cu mineralization and a late biotite alteration. The K-feldspar alteration occurs as replacement, with an assemblage consisting of K-feldspar and minor quartz, with magnetite, chalcopyrite and pyrite disseminated and in

Table 1

Lithostratigraphy and tectonic events in the San Rafael Massif (after Japas et al., 2013, 2021; Cingolani, 2017). Age data from the Choiyoi volcanics are from Rocha-Campos et al. (2011).

Time	Units			Rock sequence	Cycle	Tectonic events
Late Cretaceous to Quaternary				Back-arc magmatism & continental deposits	Andean	Andean Orogeny
Triassic	Puesto Viejo Fm ~ 241–235 Ma			Synrift-continental successions Alkaline and bimodal magmatism	Gondwanan	Rifting
Permian	Late	Choiyoi	Upper Choiyoi	Cerro Carrizalito Fm ~ 252 Ma Quebrada del Pimiento Fm Agua de los Burros Fm ~ 265 Ma	Volcanic sequence (post-orogenic silicic magmatism)		Post-San Rafael Extension (transtension)
	Early		Lower Choiyoi	Cochicó Group ~ 281 Ma	Volcano-sedimentary sequence (arc magmatism)		San Rafael Orogeny (transpression), second and first stages
Carboniferous Mesoproterozoic to Devonian	El Imperial Fm			Foreland deposits Post-collisional magmatism Passive- to active-margin deposits Metamorphic and igneous rocks	Famatinian Grenvillian	Chanic Ocloyic

veinlets. There are two types of veinlets associated with this alteration stage (Type A and B following the classification of Gustafson and Hunt, 1975). A-type veinlets have mosaic or granular texture and are composed of quartz ± chlorite ± chalcopyrite ± magnetite with localized K-feldspar selvages. B-type veinlets consist of quartz + pyrite ± chalcopyrite ± molybdenite and very scarce bornite with or without K-feldspar selvages. The late biotite alteration occurs as replacement overprinting the propylitic alteration, and in EB veinlets (following the classification of Gustafson and Quiroga, 1995) composed of biotite ± quartz with or without K-feldspar selvages. The late alteration stage includes an early low-temperature phyllic and a late carbonate alteration sub-stage. The phyllic sub-stage is irregularly distributed in the San Pedro Porphyry and the surrounding pyroclastic rocks and occurs pervasively and in D-type major veins and veinlets (following the classification of Gustafson and Hunt, 1975). The rocks affected by pervasively phyllic alteration have a white to ocher-yellowish color and a saccharide texture and a mineral assemblage composed of sericite (a mixture of illite, smectite, and Fe-chlorite determined by short wave infrared spectrometry), quartz, and minor rutile, with disseminated pyrite and minor chalcopyrite, sphalerite, and galena. In the San Pedro Porphyry, sericite along with Fe oxides partially to completely replaced plagioclase whereas biotite was partially replaced by illite, rutile and Fe oxides. The groundmass shows very strong sericitic alteration and silicification in patches. In the pyroclastic rocks, sericite completely replaced the plagioclase crystals while biotite is completely replaced by illite, Fe oxides and rutile, and amphiboles are completely replaced by Fe oxides. The matrix was partially replaced by sericite aggregates and mosaic silica. D-type major veins (*La Julia, San Eduardo, San Pedro, Sin*

Nombre and La Salvadora, Fig. 2b) occur within or close to the San Pedro Porphyry and are up to 1 m thick with selvages composed of illite-(smectite) and scarce quartz and pyrite veinlets. Ore parageneses of these major D-veins are shown in Table 2. D-type veinlets consist of pyrite ± quartz with scarce chalcopyrite, galena and sphalerite, and illite and Fe-chlorite selvages (Gómez, 2013; Gómez et al., 2015). Based on vein orientation and timing, two D-vein and veinlet systems were recognized (Japas et al., 2021): an early WNW- & ENE-trending system (D_1) and a late NNE- & ~NS-trending system (D_2; see Table 2). Finally, the late carbonate alteration sub-stage is widely distributed in the area occurring as replacement and in-veinlets, with an assemblage of calcite ± quartz ± hematite.

Stress conditions during the formation of the San Pedro porphyry copper deposit veins are shown in Fig. 3. From A to D_2 veins, differential stress decreases revealing the San Rafael orogeny decline, whereas the observed vertical stress decrease indicates progressive exhumation. The significant contribution of fluid hydrothermal pressure to hydraulic fracturing and hydraulic reactivation of fractures is also explained in Fig. 3.

Fluid inclusion data show that typical early, high-temperature magmatic fluids (up to 685 °C, 81.3 wt% equiv. NaCl; see Gómez et al., 2021) evolved to lower-temperature, moderately saline fluids (up to 454 °C, 52.4 wt% equiv. NaCl; see Gómez et al., 2021). The declining stage of the system (D_2-veins) is characterized by primary, aqueous inclusions that represent dilution by meteoric fluids (up to 211 °C, 4.80 wt% equiv. NaCl; see Korzeniewski et al. 2012). This general decrease in temperature, salinity and depth (~3 km to 200 m) during the evolution of San Pedro porphyry copper deposit resulted from uplift probably tied

Table 2

Main San Pedro district D-vein systems. Vein trends, ore mineralogy and physico-chemical conditions of primary fluid inclusions during the phyllic sub-stage (for more information see Korzeniewski et al., 2012, and Japas et al., 2021). *San Pedro* D_1-vein has no minerals suitable for fluid inclusion analysis. Abbreviations: sph: sphalerite; ccp: chalcopyrite; cc: chalcocite; ga: galena; tnt: tennantite; ttr: tetrahedrite; qzt: quartz; cb: carbonate; bn: bornite; py: pyrite; str: stromeyerite; hem: hematite; mlc: malachite; az: azurite; ccl: chrysocolla; mol: molibdenite. Alteration, Pot: potassic; Phy: phyllic; Carb: carbonate alteration.

| D-major veins		Main vein trend	Ore paragenesis and gangue	Alteration	Th (°C)	Salinity (eq.wt %NaCl)	Estimated presure (bar)	Minimum depth (m)
D_2	La Salvadora	NNE & ~NS	ga+cc+Ag native+ccp+bn+(ttr)(str)+(sph)+(hem)+qtz+cb	Phy+Carb	211 to 176	4.80 to 0.35	19.33 to 8.83	200
D_1	San Eduardo	ENE (& NE)	ga+sph+ccp+py+qtz+(cb)	Phy+Carb	276 to 214	8.68 to 5.11	56.89 to 19.85	600
	San Pedro	ENE	mlc+az+ccl+qtz	Phy+Carb		NO DATA		—
	Sin Nombre	ENE	hem specular (py ccp)+qtz	Pot+Phy+Carb	245 to 275	3.55 to 6.45	—	650
	La Julia	WNW-NW	ccp +mol +bn +ga with tnt-ttr inclusions +qtz+ (cb) (two qtz generations)	Pot+Phy+Carb	278 to 299	10.86 to 16.53	564.3 to 777.0	800
	La Margarita	WNW	sph+ccp disease+ccp+ga(Ag)+tnt-ttr+qtz+(cb)	Pot+Phy+Carb		NO DATA		—
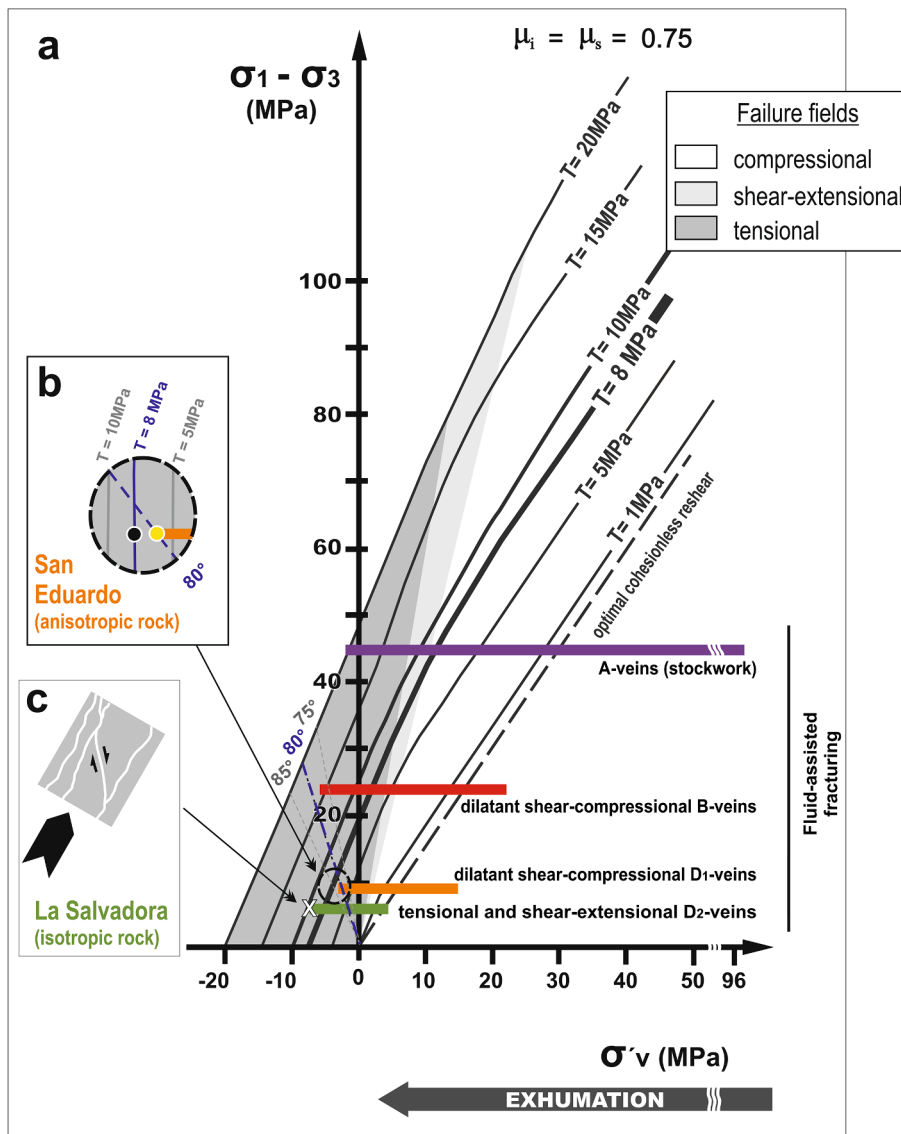
Fig. 3. Hydro-mechanical conditions of the San Pedro district main veins. a. Data from the San Pedro porphyry copper deposit veins from Japas et al. (2021) plotted into the $\sigma_1 - \sigma_3$ *versus* $\acute{\sigma}_v$ Sibsońs diagram (adapted for transpressional conditions from Sibson, 1998, 2000, and Cox, 2010). Differential stress ($\sigma_1 - \sigma_3$) represents a measure of the tectonic stress, while effective vertical stress ($\acute{\sigma}_v$) indicates the depth of fracture (vein) formation. Colored horizontal bars represent calculated stress conditions for the main veins A (magenta), B (red), D (*San Eduardo* –orange–, and *La Salvadora* –green–), revealing declining orogenic conditions, fluid overpressure and exhumation. Right end of the bars indicates dry conditions; left end of the bars reflects hydraulic fracturing of the host rock. Mechanical anisotropies also have controlled fracturing (fracture reactivation or reshearing) during some of the alteration stages (fractures hosting B- and D_1-veins). **b, c.** Data from the D-vein systems. **b.** Insert showing hydraulic fracturing at San Eduardo (D_1-vein), controlled by pre-existing fracture (reactivation). **c.** Insert outlining the newly-formed tensional and shear extensional hydraulic fractures at La Salvadora (D_2-vein) as the result of the lowering of the differential stress (see Cosgrove, 1995).

to the declining San Rafael orogenic deformation (Japas et al., 2021). Uplift, telescoping and fracture sealing due to hydrothermal sealing would have conditioned vein overprinting at the San Pedro deposit (Japas et al., 2021).

2.2. La Salvadora vein

La Salvadora vein is hosted by dacitic tuffs from the Lower Choiyoi section (Fig. 2b). The dacitic tuffs are composed of plagioclase, quartz and minor biotite and amphibole crystals in a felsitic matrix where *fiammes* and shards are occasionally recognizable. There is an alteration halo associated with this vein consisting of illite with subordinate smectite (determined by short wave infrared spectroscopy) partially replacing plagioclase, amphibole and biotite crystals and the matrix, the later also replaced by mosaic silica. This pervasive alteration is accompanied by Fe oxides and pyrite disseminated and quartz veinlets. *La Salvadora* vein corresponds to the D_2-vein system filling a braided array of steeply-dipping NNE- and ~ NS-trending tensional and shear-extensional fractures (Japas et al., 2021; Fig. 2c, 3 and Table 2). Mineralization occurs as intergrowths of galena, rhombic chalcocite, stromeyerite, native silver and occasionally tetrahedrite; myrmekitic intergrowths of galena and rhombic chalcocite; pseudo-myrmekitic

intergrowths of rhombic chalcocite and stromeyerite; intergrowths of bornite, chalcopyrite, native silver with minor sphalerite and disseminated specular hematite (Fig. 4). The gangue consists of chalcedonic quartz enclosing the mineralization and brecciated and cemented by carbonate (Rubinstein and Bevins, 2004; Table 2). Energy-Dispersive X-ray spectroscopy (EDX) analyses show that chalcocite has variable silver contents and galena is free of silver. In the oxidation zone there are abundant limonite and minor malachite, jarosite and cerussite (Rubinstein and Bevins, 2004).

Microthermometric studies carried out on fluid inclusions from vein material by Korzeniewski et al. (2012) reveal lower homogenization temperatures and salinities than those recorded in the major D_1-veins of the district (Table 2). Also, much shallower minimum formation depth was estimated by Korzeniewski et al. (2012) for *La Salvadora* D_2-vein comparing with the major D_1-veins (Table 2).

Kinematic and hydro-mechanical analyses indicate that *La Salvadora* D_2-vein was formed at the end of the phyllic sub-stage, close to the transition from the San Rafael Orogeny to the Post - San Rafael extension (Japas et al., 2021). Based mainly on (a) pressure and depth conditions provided by fluid inclusion data, (b) tensile strength values, (c) main stress-axis orientation, and (d) attitude of vein-hosting fractures, these authors determined conditions of differential stress of ~ 7.00 MPa (70
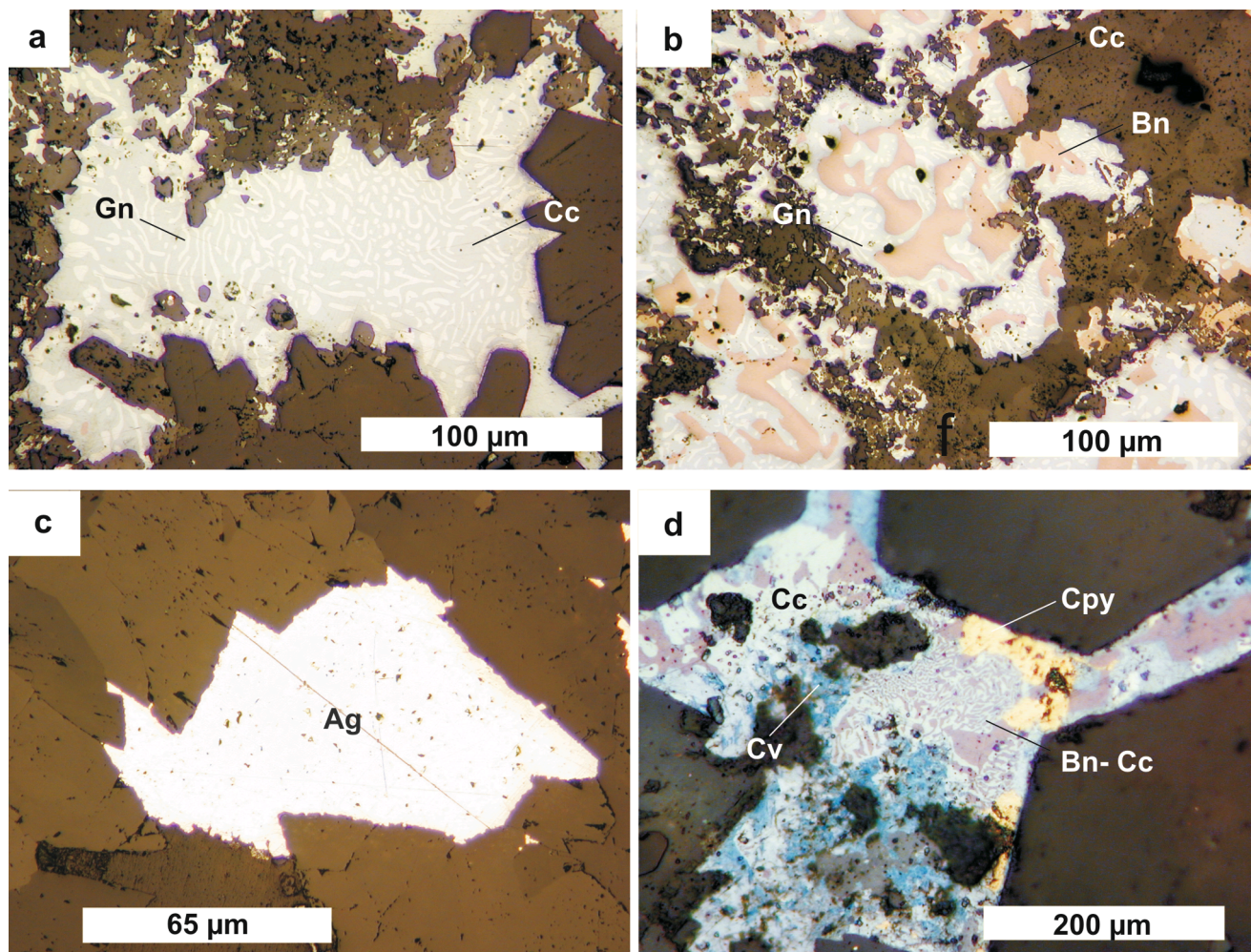
Fig. 4. Reflected light photomicrographs of *La Salvadora* D$_2$-vein ore. a. Myrmekitic intergrown between chalcocite and galena. **b.** Bornite and myrmekitic intergrown between chalcocite and galena. **c.** Native silver is commonly found as discrete grains. **d.** Myrmekitic intergrown between chalcocite and bornite. Chalcopyrite crystals and covellite patches. Abbreviations: Cpy: chalcopyrite, Ag: native silver, Gn: galena, Cc: chalcocite, Cv: covellite, Bn: bornite.

bars), hydrostatic fluid pressure of 1.93 MPa (~20 bars), and transient fluid pressure of ~ 11.00 MPa (110 bars). This transient overpressure produced hydraulic fracturing of host rock at the *La Salvadora* vein area, and would have been the result of permeability reduction by hydrothermal sealing of fractures, chemical and thermal expansion, as well as exhumation (Peacock et al., 2017; Japas et al., 2019, 2021). Hydrothermal sealing occurred immediately after D$_1$-veins formed, sealing all the previous weakness surfaces and hindering fluid circulation and escape, with the consequent increase of fluid pressure. Under these conditions, exhumation should have preserved the hydrothermal fluid pressure but reduced the vertical stress (σ_v; Peacock et al., 2017 and references therein), allowing the hydrothermal fluid to reach overpressure conditions. Moreover, thermal volumetric expansion promoted by the heat supplied by the hydrothermal fluids, and chemical volumetric expansion resulting from hydrated alteration minerals replacing anhydrous minerals during phyllic alteration,. also contributed to fluid overpressure (*e.g.*, Japas et al., 2019, and references therein).

Because the host rock does not present any surface of mechanical weakness after sealing, it becomes isotropic and consequently D$_2$-veins formed following newly-formed shear-extensional and tensional fractures (Japas et al., 2021).

3. Reverse Osmosis (RO)

Membrane processes were reported as probable mechanisms forming ore deposits at relatively low temperatures, such as those related to sedimentary basins (Becker, 1892; MacKay, 1946; Magara, 1974; Spirakis, 1977; Lueth and Whitworth, 2009; Pirajno, 2009; among others), and to the hydrothermal system (MacKay, 1946; Japas et al., 2015; Maffini et al., 2017). While MacKay (1946) broadly proposed membrane processes linked to hydrothermal systems, Japas et al. (2015) demonstrated that in the case of porphyry-type deposits, RO processes can occur at physico-chemical conditions corresponding to those of the phyllic halo formation (~325°-175 °C). More recently, Maffini et al. (2017) also considered RO as a possible mechanism to explain the atypical spatial distribution of metals in some polymetallic Pb-Zn-Cu-Ag ± Au vein-type deposits formed at 320°-180 °C and linked to brittle-ductile transtensional shear zones. Instead of occurring at structurally more favorable dilation sites, the metal ore occurs preferentially associated with zones of very intense brittle fracturing where sericitic alteration is more extensively and intensively developed (Maffini et al., 2017).

Japas et al. (2015) proposed the RO mechanism to explain the metal zoning in El Infiernillo and San Pedro porphyry copper deposits in the San Rafael Massif based on differences between these two deposits as well as some discrepancies from the traditional Lowell and Gilbert (1970) model. These authors interpreted RO as a natural mineral-concentration process supported in the existence of chemical and pressure potential-energy gradients in a declining orogeny stress scenario, the presence of a membrane (phyllic alteration), and the availability of

ions/complexes (solutes) showing different relative rejection values. In the case of the D_1-veins of the San Pedro porphyry copper deposit, RO together with the presence of an anisotropic host rock would have induced Cu, Ag, Pb and Zn to concentrate preferentially along the main fractures where alteration affected the host rock during the phyllic stage (plane phyllic membrane; see Japas et al., 2015).

In this suitable scenario for membrane processes triggering, we will test RO as a viable mechanism to explain the atypical ore paragenesis in *La Salvadora* D_2-vein.

3.1. RO principles

RO, also known as hyperfiltration, is a self-activated mechanism triggered when two solutions of different concentrations are in contact through a semi-permeable membrane, with the more concentrated solution at higher pressure than the more diluted one (Ozaki et al., 2002; Fritzmann et al., 2007; Franks et al., 2009; Japas et al., 2015; Fig. 5). Favorable pressure potential-energy gradients (higher pressure in the most concentrated solution) induce the most concentrated solution to go through the membrane producing the separation of solute from solvent due to retention of solutes at the "feed" face of the membrane (Fig. 5). Therefore, to activate RO, the most concentrated solution should be forced by pressure to flow through the membrane. Solution that passed through the membrane is known as "permeate solution" (or simply "permeate") and, because of membrane retention, permeate is impoverished in solutes (ions/complexes) when compared to the original feed solution. "Membrane retention" (or "membrane rejection") refers to the restriction of passage of solute through a membrane and represents a relative measure indicating the amount of solute that does not pass through the membrane (Amjad et al., 1998). There are two types of filtration systems: dead-end and cross flow; dead-end flow involves flow perpendicular to the membrane surface, while cross flow (or tangential flow) comprises flow along the surface of the membrane (Van der Bruggen, 2018; Microdyn-Nadir, 2019). Materials such as clays, shales, siltstones, tuffs, fault-gouges, zeolites, and even dolomites and limestones are able to behave as natural semi-permeable membranes (De Sitter, 1947; Berry, 1969; Kharaka and Berry, 1973; Whitworth, 1998; Whitworth et al., 1999; Hart, 2013).

In the industry of water purification treatment and at environment temperatures, RO is used to concentrate and separate metal ions, metal complexes, aqueous salts and atomic radius particles from their solvents at the range of ~ 70–15 bars of transmembrane pressures (pressure differences at both sides of the membrane). Nanofiltration (NF) is another pressure-driven retention-selective filtration process applied to particles at the nanometer scale which operates at ~ 20–5 bars (Schäfer et al., 2002; Camarillo-Blas, 2005). It shares some similarities with RO; in fact, regarding the ionic size there is an overlapping zone between RO and NF fields (Fig. 6). Depending on the solute concentration, the required applied pressure can widen to ~ 200–10 bars for RO filtration (Rautenbach and Linn, 1996; Giwa and Ogunribido, 2012; Camarillo-Blas, 2005), and to 40 - ~3.5 bars for NF (Schirg, 2001; Ghiu, 2003; Dupont 2021). Instead of being controlled by diffusion and by solute size, as seems to be the case of RO (*e.g.,* Childress and Elimelech, 2000), NF would be influenced by the size (steric or sieve effect), electrostatic properties of the solute (Donnan effect; Donnan, 1995), and dielectric effects (Agboola et al., 2015). In the case of NF, removal of heavy metal ions requires the previous complexing of metals (Lastra et al., 2004; Rogel-Hernández et al., 2006; Murthy and Chaudhari, 2009; Abhang et al., 2013).

Size and charge of solutes affect their passage through the RO and NF membranes. According to many authors (*e.g.,* Liu, 2007), the larger the size and charge of the solute, the higher the solute rejection (that is, the lower the solute passage). As tested by Japas et al. (2015), solute retention passage seems to be dependant on the charge/mass ratio as it shows a remarkable coincidence with the measured rejection series for metal ions: the lower the solute charge/mass ratio, the lower the retention (in other words, the higher the [–log solute charge/mass ratio], the lower the retention).
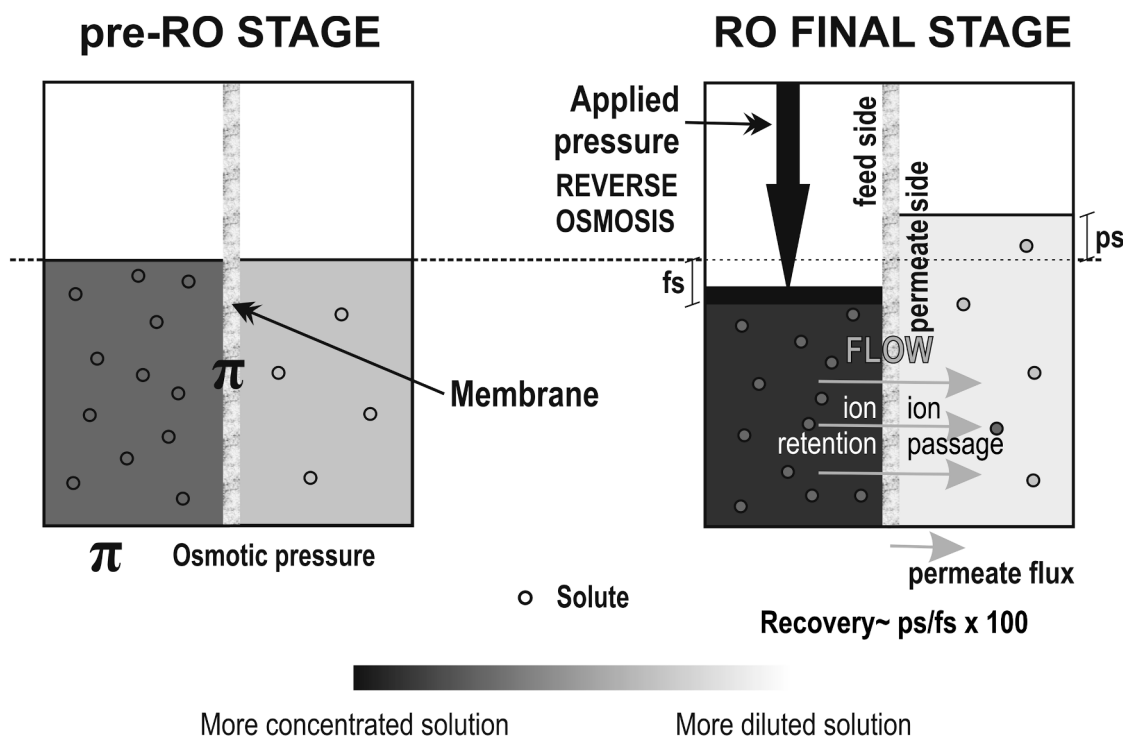

Fig. 5. RO mechanism and osmotic transport. Differences in pressure and chemical potential across a membrane enable selective transport through the membrane restricting the passage of solutes in relation to the passage of the solvent (modified from Japas et al., 2015).
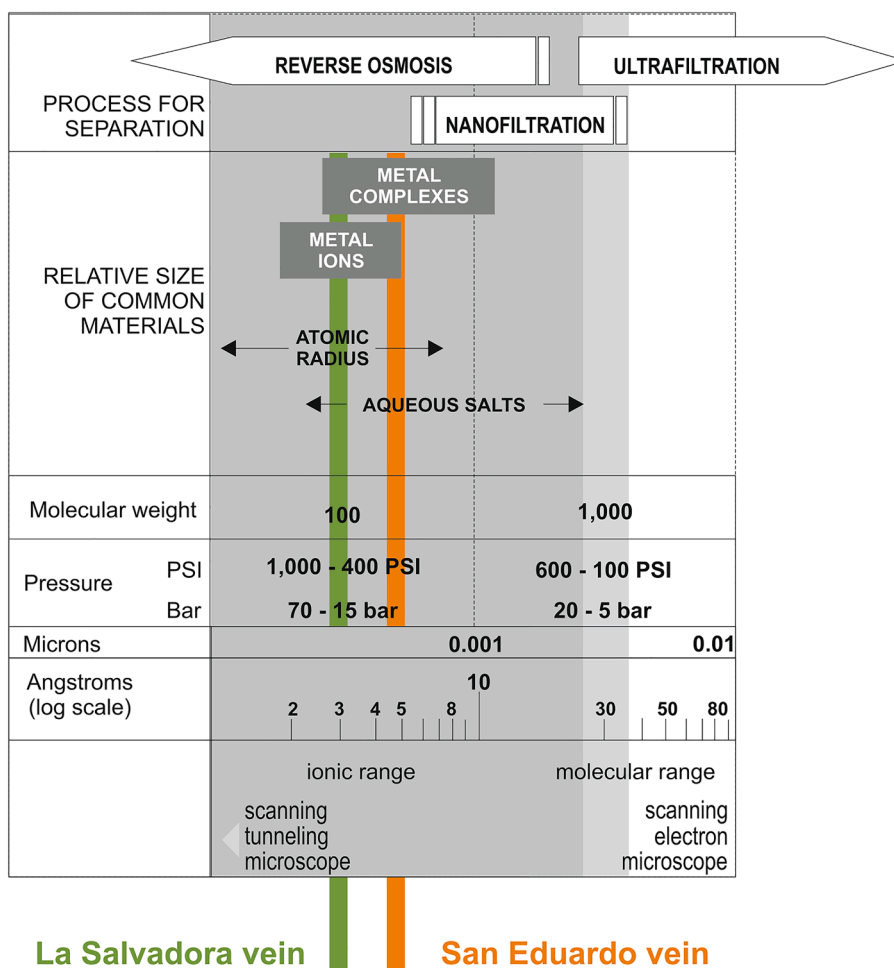
Fig. 6. Membrane separation systems and their filtration spectrum for solutes at the ionic and molecular ranges. RO and NF are size and diffusion exclusion processes (modified from Japas et al., 2015). Colored bars indicate the transmembrane pressures (see Table 4) calculated for *La Salvadora* D_2- (green) and *San Eduardo* D_1- (orange) veins using datafrom Japas et al. (2021).

3.2. Factors controlling RO performance

The mechanisms of ion transport during solute separation from the solvent in the membrane are poorly known. Most of the RO and NF knowledge (*e.g.,* membrane performance, separation mechanisms) are empiric and arises from direct experimental methods which allow to define the most critical conditions; theoretical methods try to improve the understanding of experimental results through predictive mathematical models. These predictive models (*e.g.,* the Kimura-Sourirajan model, describing solute transport by diffusion; the Spiegler-Kedem

Table 3
Synthesis of factors controlling RO performance (recompiled from the industry and scientific literature). M: Membrane; FW: Feedwater; F/R: Factor/Retention relation

FACTOR		F/R	COMMENTS
M	Pore size	**inverse**	
	Charge	**direct**	
	Thickness	**(direct)**	
	Hydro-character	**variable**	Hydrophilic membrane, $>$ change with pH
			Hydrophobic membrane, $<$ change with pH
F W	Solute Size	**direct**	
	Solute Charge	**direct**	
	Temperature (T)	**inverse**	$>$ T, $<$ pressure to produce flow
			$>$ T, $>$ permeate
	Operating time	**inverse**	Fouling & scaling
	Transmembrane pressure (TmP)	**direct**	$>$ TmP, $>$ permeate flux
	pH	**variable**	**Membrane:** lower retention at ZPC = IEP
			Solute: affects charge, size and solubility
	Feed concentration (FC)	**inverse**	$>$ FC, $>$ pressure required to produce flow
			$>$ FC, $>$ permeate concentration
			$>$ FC, $<$ permeate flux
	Flow rate (FR)	**(direct)**	$>$ FR, $<$ permeate concentration
			$>$ FR, $>$ permeate flux

model, considering salt transport due to diffusion and convection; among others; Ghiu; 2003; Agboola et al., 2015, and references therein) are conceptually different, and show a variable degree of acceptance in the membrane scientific community.

Retention of solutes by RO and NF is conditioned by characteristics of the membrane and the feed water (Table 3; Bartels et al., 2005). Regarding the membrane, the most important factors conditioning filtration are pore size and charge. Membrane thickness and the hydrophilic (attract water molecule)/hydrophobic (repel water molecule) character of the membrane also influence the filtration performance (Szoke et al., 2002; Mänttäri et al., 2006).

On the other hand, feed water factors influencing solute retention and consequently permeate flux are: temperature, operating time, transmembrane pressure, pH, feed concentration and flow rate (Al-Alawy and Salih, 2017; see also Japas et al., 2015 and references therein). Some of these factors show some degree of interactions. Temperature of feed water plays a main role in RO efficiency because at lower temperatures, solute retention increases and permeate flow decreases while the required operating pressure to produce flow is higher (see Hawlader et al., 2000; Al-Mutaz and Al-Ghunaimi, 2001; Emalsa, 2007; Japas et al., 2015). RO membrane performance usually decreases with time since both, particulate matter and precipitate inorganic material tend to harm it. These damages are referred in the specific scientific and industry literature as "fouling" and "scaling", respectively (Freeman and Majerle, 1995; Fritzmann et al., 2007; Jarusutthirak et al., 2007; among many others). A decrease in solute rejection and in recovery (percentage of the feed solution that emerges as permeate solution) represents the main consequences of fouling and scaling (see Japas et al., 2015 and references therein). Transmembrane pressure controls permeate flux across the membrane (the higher the transmembrane pressure, the higher the flux; *e.g.,* Lanxess 2013), and therefore affects retention and fouling. Effectiveness of RO and NF filtration changes with the pH of the feed solution (Hagmeyer and Gimbel, 1998; Childress and Elimelech, 2000; Ozaki et al., 2002; Tanninen and Nyström, 2002; Franks et al., 2009; Al-Alawy and Salih, 2017; among others). Laboratory testing and field performance show that an increase in pH produces changes in charge, size or solubility of some of the constituents in the feed solution, and also influences the RO membrane charge (Hagmeyer and Gimbel, 1998; Childress and Elimelech, 2000; Ozaki et al., 2002; Qin et al., 2005; Franks et al, 2009; Lanxess 2013). The two relevant parameters conditioning the membrane charge are the Zero Potential Charge (ZPC) and the Isoelectric Point (IEP). The ZPC represents the pH value at which the net total particle charge is equal to zero (Sposito, 1989) whereas, the IEP corresponds to the pH value at which the zeta potential is zero, being the zeta potential the potential of the surface and adsorbed species (see Cristiano et al., 2011). When there is no adsorption of other ions than the potential determining H+/OH– at the surface, ZPC = IEP. Dependent on the ZPC and/or the IEP, RO and NF membranes are positively and negatively charged below and above this pH value, respectively (Hagmeyer and Gimbel, 1998; Childress and Elimelech, 2000; Ozaki et al., 2002). According to Ozaki et al. (2002), at pH values in which solid membrane particles are electrically neutral (ZPC condition), the membrane shows its lowest rejection value; in most of the membranes, ZPC is usually reached at pH = 4–5. Experimental data from Ozaki et al. (2002) has also shown that changes in the charge property of surface material in ultra-low-pressure RO membranes affect rejection and flux of heavy metals. Regarding flow rate, recent experimental work by Al-Alawy and Salih (2017) confirms previous results obtained by Hawlader et al. (2000), Emalsa (2007) and Filmtec (2012), proving that during rising flow rate, a decrease in permeate concentration and an increase in flux occurred. Conversely, an increase in feed solution concentration should decrease flux and rejection, and should increase permeate concentration (Filmtec, 2012).

Although all these tests were performed using synthetic organic membranes, we interpret that these results may also apply in natural inorganic membranes assuming their similar electrostatic and pore size

constraints. Differences between inorganic and organic membranes include: extended performance at higher pressures, wider pH and temperature range conditions, as well as higher mechanical and chemical resistance, and higher fouling capacity for inorganic membranes (Palacio-Martínez, 1998; Li et al., 2016; Llorente-Ayza, 2017; Azaman et al., 2021).

With this in mind, and because the main physico-chemical differences between D_1- and D_2-veins at San Pedro district are linked to temperature, transmembrane fluid pressure and feed solution concentration (i.e., salinity; Japas et al., 2021; see Table 2), we will test these conditioning factors to assess RO viability in explaining ore paragenesis of *La Salvadora* vein.

4. Metal zoning at the San Pedro porphyry copper deposit

Metal concentration during the phyllic alteration sub-stage is relevant to check the proposed link between metal zoning and membrane processes.

Metal anomaly distribution maps were constructed based on 274 chemical analyses of chip rocks and chip channels in the exposed alteration zones by Portal Resources Ltd. (Fig. 7a-d). Database from Davicino (2008) was processed following descriptive statistics. Background and threshold values were calculated for each element following Lepeltier (1969) for log normal distributions.

Surface geochemical analyses reveal a main Cu anomaly that overlaps with the potassic and phyllic alteration zones whereas Pb-Ag anomaly is linked with *La Salvadora* and *San Eduardo* D-veins (Fig. 7). The Zn content is abundant mostly at the potassic alteration zones but is also present at *La Salvadora* and *San Eduardo* vein systems (Gómez, 2013).

A comparative metal content test to investigate the possible incidence of Chemical Oxygen Demand of the media (COD) on the osmotic behavior of Zn during the phyllic alteration in San Pedro deposit is also presented; being COD a measure of the capacity of the solvent to consume oxygen during the oxidation of inorganic chemicals (Chianese et al., 1999). Because the data range embraces several orders of magnitude, metal content data from Davicino (2008) is plotted in a compact way using logarithmic representations (Fig. 8). From the nine plots made for the *San Pedro*, *San Eduardo*, *La Salvadora* D-veins (log Zn *vs.* log of Cu, Ag, Pb), only the two shown in Fig. 8 reveal a valuable correlation ($R^2 \geq 0.7$).

5. Estimation of physico-chemical conditions during D-vein formation in the RO context

Physico-chemical data of the phyllic sub-stage in San Pedro porphyry deposit will be presented in this section and compared with those of the RO mechanism scenario, with the aim of testing a possible link between ore paragenesis of *La Salvadora* D_2-vein and RO mechanism.

5.1. Transmembrane pressure

At *La Salvadora* and *San Eduardo* D-veins, the significant transmembrane pressure is the result of the hydrothermal fluid pressure surpassing the stress normal to the fracture walls (σ_n), which is equal or close to the minimum stress σ_3 (Fig. 9). Calculations using data from Japas et al. (2021) allow to define transmembrane pressure conditions during the formation of *La Salvadora* (D_2) and *San Eduardo* (D_1) veins in ~ 60 and ~ 40 bars, respectively (Fig. 9 and Table 4).

5.2. Metal rejection as a function of temperature

As mentioned in section *3.2*, temperature of the feed solution strongly affects membrane performance. According to Hawlader et al. (2000) solute passage increase per °C is slightly less than 2%.

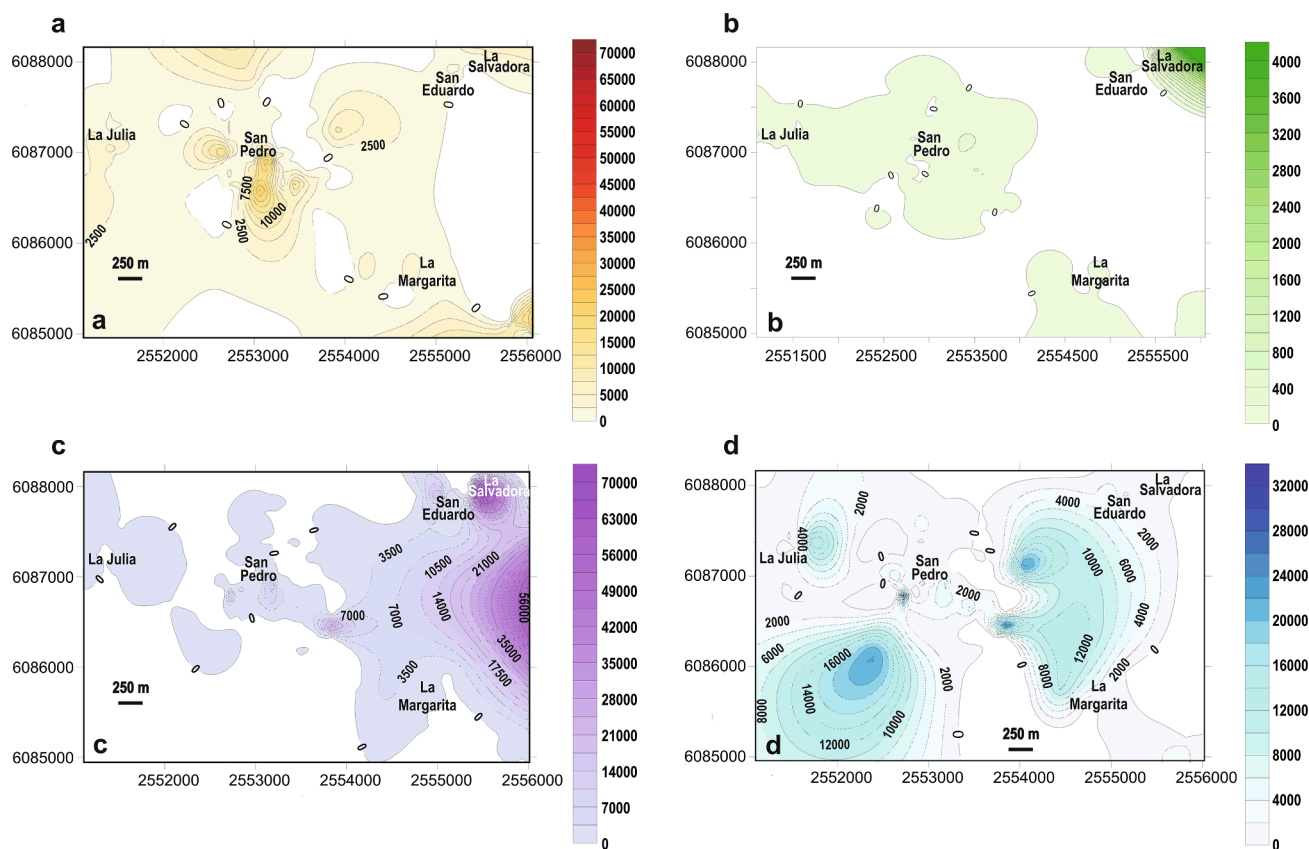Fig. 10 shows the variation of solute passage for Cu^{2+}, Zn^{2+}, Ag^+ and

Fig. 7. Surface geochemical anomalies in the San Pedro district. Maps show the spatial distribution of metal elements in the San Pedro porphyry copper deposit area (after Gómez, 2013). Curves represent the metal contents (in ppm) for **a.** Cu, **b.** Ag, **c.** Pb, **d.** Zn, Veinlets and stockworks were not considered in the statistic analysis as they were considered outliers (Gómez, 2013). Gauss-Krüger coordinates.
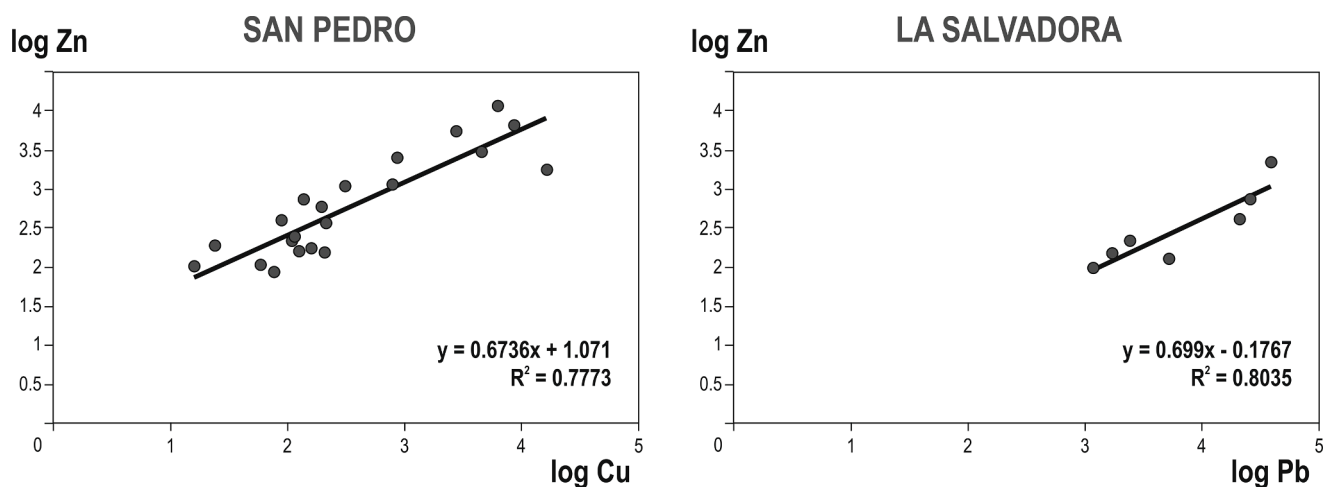

Fig. 8. Geochemical data logarithmic plots from the phyllic alteration affecting the *San Pedro* and *La Salvadora* D-vein areas to individualize similarities or differences between osmotic behavior of Zn and the other metals (data from Davicino, 2008). The Zn content indicates higher affinity to Cu^{2+} in *San Pedro* D_1-vein case, and to Pb in *La Salvadora* D_2-vein case. The higher COD for D_1-vein than for D_2-vein fluids explains the different osmotic behavior of Zn during D_1- and D_2-vein formation.

$Pb^{2+/4+}$ (simplified as Cu, Zn, Ag, and Pb) as a function of temperature during RO process, considering different correction factors close to the 2% value defined by Hawlader et al. (2000). The temperature ranges of *La Salvadora* and *San Eduardo* D-veins obtained from fluid inclusion studies performed by Korzeniewski et al. (2012) are plotted (Fig. 10).

Considering the most common solute passage SP values at 25 °C and a rejection incremental rate of 2% per °C, Ag, Pb, Cu and Zn will be retained on the membrane feed side at temperatures $\leq$ 170 °C (reference bar I in Fig. 10a). At temperatures between 175 °C and 200 °C, Ag and Pb could be practically removed depending on the membrane type, while Cu and Zn will be still retained (reference bar II; Fig. 10a). At temperatures between 200 °C and 260 °C, only Cu and Zn will be retained (reference bar III; Fig. 10a), and at temperatures higher than 260 °C, nor Ag/Pb neither Cu/Zn will be retained by the membrane (reference bar
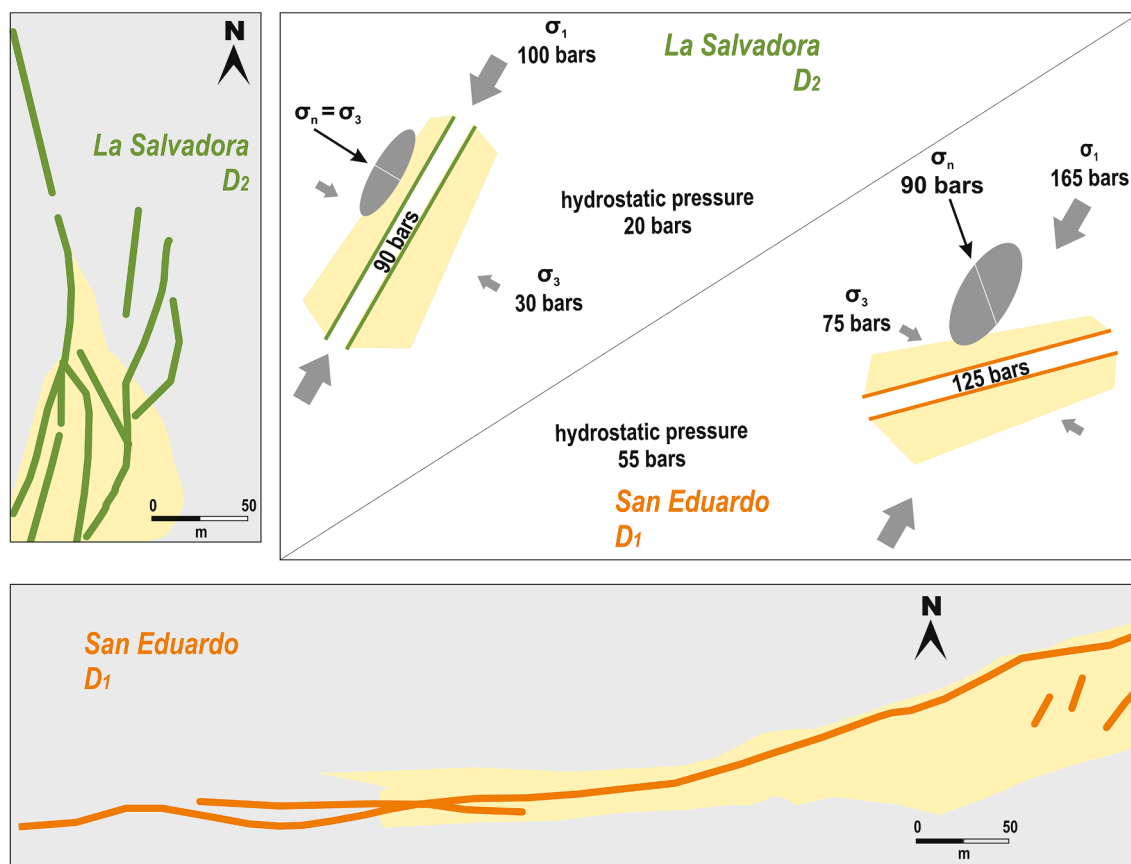
Fig. 9. Pressure gradient conditions for *La Salvadora* and *San Eduardo* D-vein cases. Pressure conditions indicating hydrothermal fluid pressure exceeding the tectonic pressure.

IV; Fig. 10a).

When applying the correction factor of 1.5% per °C instead of 2%, it can be seen that the temperature interval for an osmotic differentiation mechanism expands (225°-330 °C) and enhances the osmotic differentiation range of solutes (Fig. 10a and c).

Fig. 10 shows that at increasing temperatures, SP increases and that there are no membrane effects at temperatures higher than 260 °C (correction factor of 2% per °C), 290 °C (correction factor of 1.75% per °C), and 330 °C (correction factor of 1.5% per °C). Therefore, the 260°-330 °C temperature represents the maximum temperatures constraining the existence of osmosis-related differentiation according to the correction factor, indicating that at higher temperatures all the considered metal solutes would go through the membrane.

5.3. Chemical Oxygen Demand

For most of the metals, the influence of the COD on their passage coefficient is negligible, but Zn passes through more readily at higher COD of the stream (Chianese et al., 1999). This dependence of Zn passage to the COD could then explain why Zn can concentrate in polymetallic veins (*e.g.*, El Infiernillo deposit) and/or can overprint the Cu-enriched potassic cores (see Sillitoe, 2010). Thus, the osmotic behavior of Zn could change from similar to Cu^{2+} (relative low COD) to more akin to Ag^+ and Pb (relative high COD; see Japas et al., 2015).

Indirect values of COD of the stream can be obtained via Eh conditions. The Eh values for the D-veins were roughly estimated based on data from assemblage stability of sulfides in aqueous solutions (Sato, 1992), and the pH values for the phyllic alteration conditions (Corbett and Leach, 1997). For the *San Pedro* and *San Eduardo* D_1-veins, Eh would be $\sim$ -0.50 to -0.70 V, whereas for the *La Salvadora* D_2-vein, $\sim$ -0.2 to -0.35 V (Fig. 11). Comparing the obtained Eh conditions of these vein

ores, it can be extrapolated that fluids precipitating ore in *La Salvadora* D_2-vein should have been relatively more oxidized than in *San Pedro* and *San Eduardo* D_1-veins.

5.4. Rejection series for metal chloride complexes

There is not a complete rejection dataset for all the chemical solutes present in porphyry-type deposits, since available information about metal ion rejection is restricted to those present in wastewater, leachate and seawater. Nonetheless, considering that there is a theoretical relationship between the degree of rejection and the charge/mass ratio for metal ions (Table 5a; Japas et al., 2015) it is possible to estimate the relative rejection of metal complexes using this ratio (see Supplementary Table 1a).

Supplementary Table 1b lists the charge/mass ratio for the most common Cu, Ag, Pb and Zn chloride complexes coexisting in the hydrothermal system (*e.g.,* Seeward et al., 2013; Mei et al., 2013, 2014, 2015). When ordered following an increasing [–log solute charge/mass ratio], a decreasing solute retention series can be obtained (see section *3.1,* Table 5b).

6. Discussion

As previously mentioned, the physico-chemical conditions required to activate membrane processes are compatible with those of the porphyry system environment. The presence of two solutions showing different concentration/salinity is represented in the porphyry environment by (1) fluids exsolved from the magma and transporting metal complexes and (2) diluted connate/meteoric waters. Both solutions are separated by a natural planar membrane consisting of the phyllic-altered fracture walls (Japas et al., 2015). Following these authors, all the

Table 4
Transmembrane pressure. Calculated transmembrane pressure for *La Salvadora* and *San Eduardo* D-veins based on data from Japas et al. (2021), which are referred with (*).

	Differential stress * (bars)	Principal stresses * (bars)	Fluid pressure * (bars)	Hydrostatic fluid pressure * (bars)	Hydrothermal fluid pressure * (bars)	Trans-membrane pressure (bars)
La Salvadora	70	$\sigma_1 \approx 100$ $\sigma_2 = 50$ $\sigma_3 \approx 30$	110	20	90	(90–30) = **60**
San Eduardo	90	$\sigma_1 \approx 165$ $\sigma_2 = 150$ $\sigma_3 \approx 75$	180	55	125	(125–90) = **40**

physico-chemical factors should result in fluid transport from the magmatic source outwards through the membrane, inducing (a) the restrictive passage of solutes in relation to the passage of solvent, (b) the selective transport of solutes based on their relative membrane retention/rejection values, and (c) the dilution of the permeate solution. In addition, the temperature gradient between feed hydrothermal and connate solutions, and the presence of illite (hydrophobic mineral) would have also enhanced this osmotic transport direction (thermal-osmosis; Villaluenga et al., 2006; see Japas et al., 2015).

Data from *La Salvadora*, *San Eduardo* and *San Pedro* D-veins will be compared and discussed in this section to evaluate the RO mechanism as responsible of metal zoning during the phyllic alteration sub-stage. These D-veins were selected because they only display phyllic alteration (Gómez, 2013), and fluid inclusion and paragenesis data are available.

6.1. Pressure in the RO mechanism context

The hydrothermal/tectonic pressure conditions during *La Salvadora* and *San Eduardo* vein formation (~60 and ~ 40 bars, respectively; Table 4) is consistent with the pressure range necessary to trigger RO (70–15 bars; Fig. 6). The relatively higher pressure at *La Salvadora* D_2-vein case (~60 bars) correlates with the premise of the need of higher pressure to produce permeate flow at lower temperatures, in other words, to activate RO (Al-Mutaz and Al-Ghunaimi, 2001; Emalsa, 2007; Hawlader et al., 2000). Moreover, and as mentioned in section *3.2*, the higher the pressure the higher the retention and the permeate flow, confirming that pressure and solution concentration gradient would have conditioned RO performance at *La Salvadora* D_2-vein case.

6.2. Rejection of metal complexes and COD constraints

It can be seen in Table 5b that the Ag and Pb chloride complexes show the lowest retention values, as in the case of considering the individual metal ions (section *5.4*, and Table 5a), because the magnitude of the charge is very significant in defining the charge/mass ratio. This would support an equivalent analysis for the metal chloride rejection (relative and not absolute) as a function of temperature than that of Fig. 10 (see next section).

Within the metal chloride complexes, those of Ag^+ and Cu^+ are more stable (higher logK; Table 5b), and show a similar relative lower [–log solute charge/mass ratio], meaning that they will be, if present, commonly associated, as it is the case of *La Salvadora* D_2-vein (Table 2). The higher [–log solute charge/mass ratio] of the monovalent Cu^+ than the divalent Cu^{2+} results in an osmotic behavior of Cu^+ similar to Ag^+, explaining therefore the exclusive presence of Cu^+ in the *La Salvadora* D_2-vein.

As mentioned in Section 5.3, experimental work showed that COD would control the osmotic behavior of Zn; at high COD values, rejection of Zn should be lower showing therefore a stronger affinity to Pb and Ag, while at low COD values, the osmotic behavior of Zn should be similar to Cu^{2+}. At the *San Pedro* D_1-vein area, Zn shows higher affinity to the Cu^{2+} content (Fig. 8). Conversely, data from *La Salvadora* D_2-vein area indicate a good correlation between Zn and Pb content, and weak correlation between Zn and Cu (Fig. 8). Although not entirely conclusive, the obtained results suggest a scenario which is consistent with an operating RO mechanism.

### 6.3. Rejection variation linked to declining temperature conditions

Fig. 10 reveals that (1) at higher temperatures, rejection contrast increases between different metal ions leading to osmotic differentiation, and (2) this osmosis-related differentiation would be effective at temperatures that are consistent with those of the phyllic sub-stage of the San Pedro porphyry copper deposit.

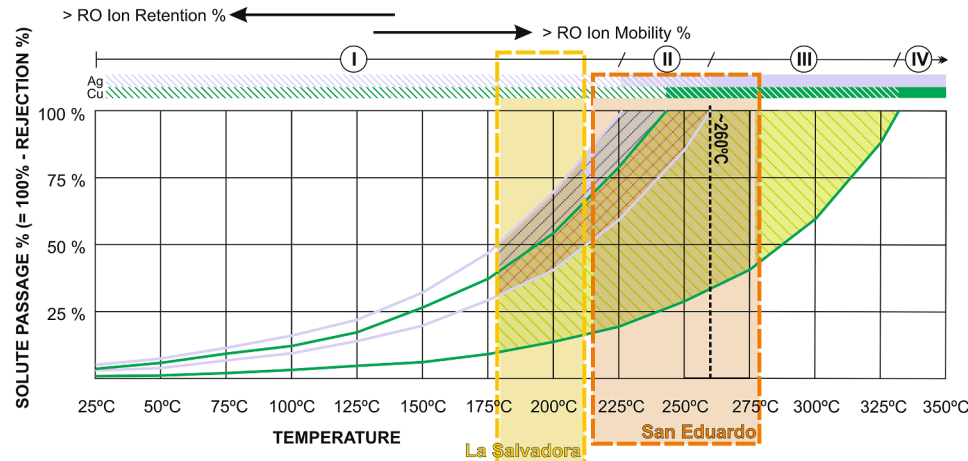The compatibility of the range of the modeled temperatures and the
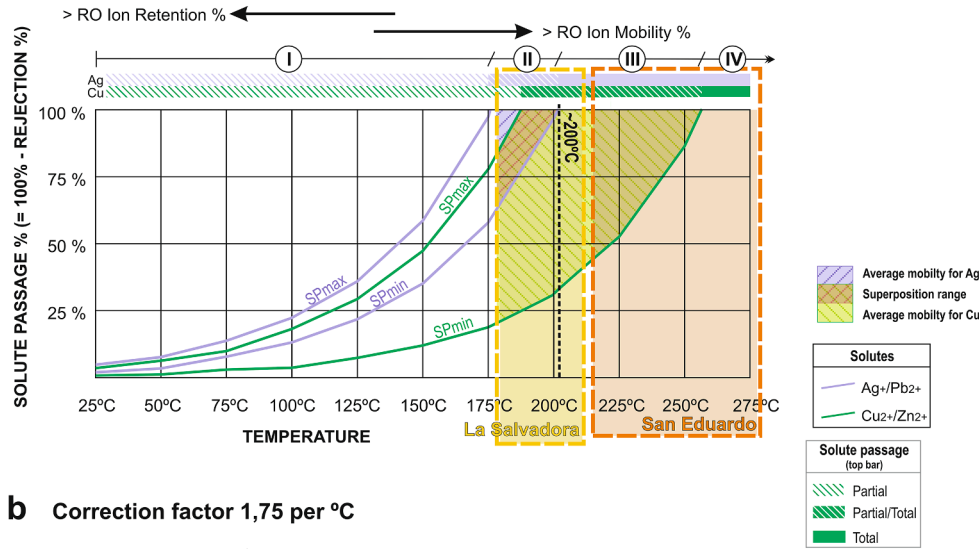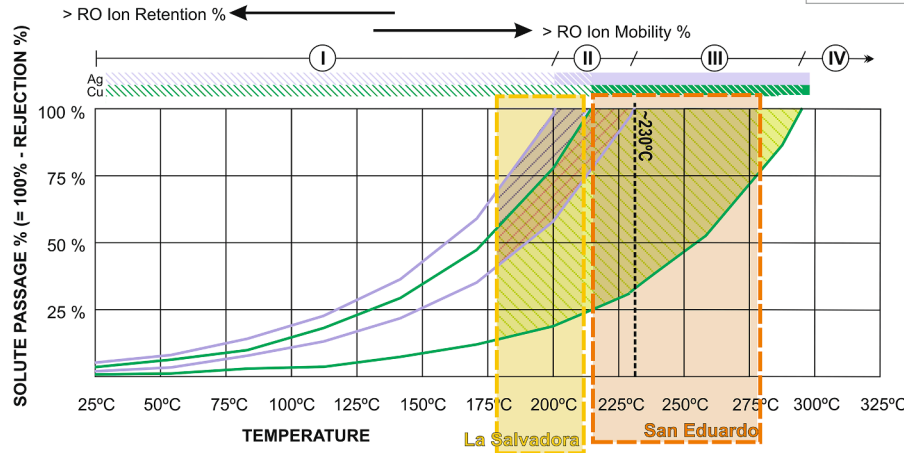
Fig. 10. RO and solute passage (SP) for different temperatures considering thermal correction factors of (**a**) 2% per °C, (**b**) 1.75% per °C, and (**c**) 1.5% per °C (modified from Japas et al., 2015) to show the degree of variation of curves according to the correction factor value. Two curves for Cu and Zn, and two for Ag and Pb refer to the minimum solute passage SP_{min} and maximum solute passage SP_{max} values each other. They are constructed based on the intervals of solute passage values available from the industry literature for 25 °C, and expanded to 325 °C following Japas et al. (2015) by using the correction factor defined by Hawlader et al. (2000). Reference bar I: temperature range for Ag, Pb, Cu, Zn retention; reference bar II: temperature range for partial Ag and Pb removal, and Cu and Zn retention; reference bar III: temperature range for exclusive Cu and Zn retention; reference bar IV: temperature range without Ag, Pb, Cu, Zn retention. Zn retention depends also on COD. Notice that for lower temperatures it should be more feasible the coexistence of Cu and Ag sulfides because of their similar passage values SP. Rectangles refer to the temperature range for the *San Eduardo* D_1-vein and *La Salvadora* D_2-vein systems, based on fluid inclusion data by Korzeniewski et al. (2012); the consistency with the relative metal content shown per vein area is noticeable.

conditions for RO selective filtration activation is also supported by the occurrence of illite, which indicates a maximum temperature of $\sim$ 325°-360 °C (Cathelineau, 1988; Rosenberg, 2002); the presence of chalcopyrite in some of the D-veins which denotes temperatures of 200 °C to < 335 °C (Reed and Palandri, 2006); and the temperatures reported for the phyllic sub-stage in the San Pedro porphyry deposit (276°-176 °C;

Korzeniewski et al., 2012).

Comparing the temperature spectrums in Fig. 10, it is found that the coexistence of Cu, Zn, Ag and Pb should be more viable at lower temperatures, because of the highest mobility (lower rejection) of Ag and Pb at higher temperatures. These plots also reveal that at the temperature range recorded in *La Salvadora* D_2-vein (211°-176 °C; Fig. 10), Ag should
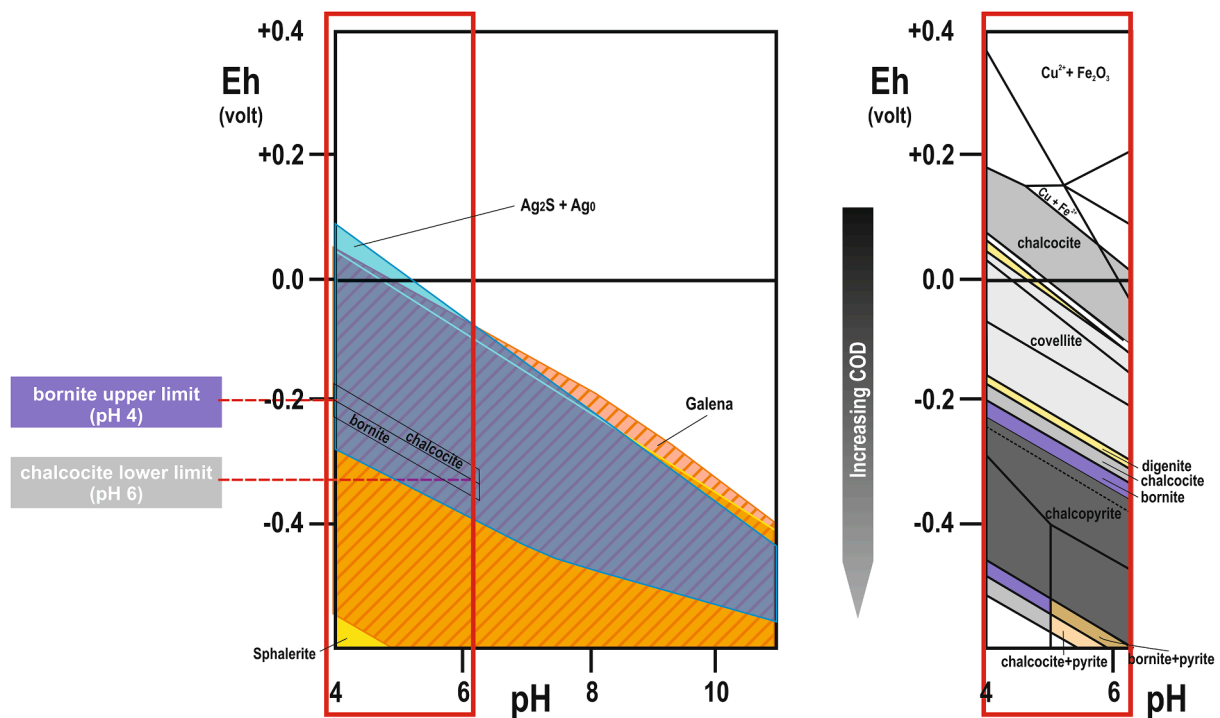
Fig. 11. Pourbaix diagram and Chemical Oxygen Demand (COD). Persistency field Eh - pH diagrams for assemblage stability of sulfides (supergene) at 25 °C and 1 bar (adapted from Sato, 1992). Two plots are presented to facilitate comprehension: left plot shows persistency field Eh - pH diagrams for Zn, Pb and Ag sulfides; right plot, composite stability Eh – pH diagram for Cu-Fe-S-O–H.

be retained by the phyllic membrane with Cu. Therefore, Ag and Cu should precipitate together due to metal concentration at the feed side of the membrane, that is, within *La Salvadora* D_2-vein.

As a result of the filtration effect of the phyllic membrane at higher temperatures Cu concentration in *San Eduardo* D_1-vein should be much more significant relatively to Ag than in *La Salvadora* D_2-vein (Fig. 10) which is reflected in the ore mineralogy (Table 2). Besides, at higher temperatures, Ag should undergo lower retention/rejection, and therefore, temperature conditions during D_1-vein formation would promote higher osmotic differentiation of Cu^{2+} (and Zn) and Ag/Pb resulting in ore paragenesis with significant Cu^{2+} ores (*San Eduardo* D_1-vein; Table 2). Conversely, temperature conditions during *La Salvadora* D_2-vein formation should induce a lower osmotic differentiation of Cu (and Zn) and Ag/Pb, leading to this atypical Ag-bearing ore paragenesis (Fig. 10). The dominant presence of Cu^+ sulfides in *La Salvadora* D_2-vein paragenesis (chalcocite) agrees with the similar Cu^+ and Ag^+ chloride complex charge/mass ratio (Table 5b; Japas et al., 2015). Additionally, and even though *La Julia* D_1-vein data was not considered in this analysis because it reactivates a B-vein from the potassic alteration stage, it results notable that the temperature of the D_1-vein formation also agrees with an ore paragenesis dominated by Cu^{2+} sulfides.

Table 5b lists the metal chloride complexes according to their increasing [–log solute charge/mass ratio], and consequently, decreasing retention. This series is similar to that for the metal cations (Table 5a), both showing lower retention values for Ag and Pb than for Cu (Cu^{2+}) (and Zn). Therefore, the retention series for metal chloride complexes can be extrapolated to higher temperatures using the same thermal correction factors and according to the calculations in Japas et al. (2015).

6.4. Rejection and pH conditions

According to Corbett and Leach (1997), pH conditions of hydrothermal fluids during the phyllic alteration should be constrained between 4 and 6. According to experimental data from Anilema-Pilamunga

and Martínez-Ortíz (2018), and from Ozaki et al. (2002) and Cristiano et al. (2011), the ZPC = IEP (zero potential of charge = isoelectric point) of illite should be at pH between 5.3 and 7. Consequently, this ZPC = IEP value would imply that during D-vein formation, retention could be linked to a positively charged membrane ($4–6 \leq 5.3–7$). In such a scenario of a charged membrane, the more charged the solutes, the more the solute retention (Ozaki et al., 2002), due to the lower [–log solute charge/mass ratio] (Japas et al., 2015).

Although experimental results by Ozaki et al. (2002) reveal that regardless of the charge of the solutes, retention increases away form the ZPC = IEP value of the membrane, Pal (2015) indicates that a positively charged membrane at pH = 4–6 will expulse co-ions (cations) and will retain anions (*e.g.,* metal chloride complexes) because of the Donnan potential effect (see Ong et al., 2002). Both experimental results support RO as a feasible mechanism operating at the San Pedro porphyry deposit.

6.5. La Salvadora vein paragenesis in the RO context

Considering (a) the lower fluid temperatures (211°-176 °C), (b) the San Rafael Orogeny declining scenario with hydrothermal fluid pressure higher than the minimum tectonic pressure or stress (stress normal to fracture wall; Japas et al., 2021), (c) the presence of illite minerals linked to phyllic alteration acting as semi-permeable barriers and (d) the presence of quartz gangue (frequent RO scaling substances), the pressure-sensitive RO mechanism could be considered as a plausible metal concentration process in the *La Salvadora* D_2-vein case. Regarding the physico-chemical conditions in which *La Salvadora* D_2-vein was formed, membrane rejection values for Cu should be similar than those for Ag (Fig. 10) inducing similar passage of Cu and Ag through the membrane, reducing therefore the higher metal osmotic differentiation that occur at higher temperatures (Fig. 10; see also Japas et al., 2015). Comparing those physico-chemical parameters constraining RO with those obtained for *La Salvadora* D_2-vein case, striking coincidences could be observed not only regarding the favourable temperature range and

Table 5

Empiric RO retention series. Empiric RO retention series for solutes based on solute charge/mass ratio (see Japas et al., 2015). **a.** Metal cations ordered following increasing the [–log solute charge/mass ratio], representing metal cation decreasing retention. **b.** Metal chloride complexes (Cx) ordered following increasing [–log solute charge/mass ratio], representing decreasing metal chloride complex retention. ch/m: charge/mass ratio. Metal chloride complexes and their K values are taken from Smith and Martell (1976). K: formation constant; it represents the complex stability (logK≪1, as is the case of the Cu^{2+}-chloride complex $[CuCl]^+$ indicates a not stable metal complex, and presence of dominant dissociated forms Cl^- and Cu^{2+}).

a	
Metal cation	**ch/m (-log)**
Cu2+	1.51
Zn2+	1.52
Pb4+	1.72
Cu+	1.80
Pb2+	2.04
Ag+	2.04

b		
Cx	**Cx ch/m (-log)**	**K (log)**
[CuCl3]2-	1.93	~ 5 a 6
[CuCl]+	1.99	~ 0
[ZnCl]+	2.00	~ 0.3
[ZnCl4]2-	2.01	~ 0.2
[AgCl3]2-	2.03	~ 6.2
[Cu2Cl4]2-	2.13	~ 13
[CuCl2]-	2.13	~ 5 a 6
[AgCl4]3-	2.19	~ 6
[AgCl2]-	2.25	~ 5
[ZnCl3]-	2.34	~ 0.5
[PbCl]+	2.38	~ 1
[PbCl4]2-	2.42	~ 1.7
[PbCl3]-	2.49	~ 2
AgCl	xx	~ 3.2
ZnCl2	xx	~ 0
PbCl2	xx	~ 1.6
CuCl	xx	~ 3

metal complexes size and charge, but also concerning transmembrane pressure conditions of ~ 60 bars that is compatible to the most common pressure range (70–15 bars) defined for RO systems operating at 25 °C, a value also comparable with those pressures recorded by the *San Pedro* and *San Eduardo* D₁-veins.

Based on the well-founded hypothesis that a charged membrane could selectively separate lighter from heavier isotopes (*e.g.,* O, Cl, Li; Fritz et al., 1987; Whitworth, 1993; Fritz and Whitworth, 1994; Whitworth, 1998), future research work focusing on isotope fractionation, and its incidence to redox controls, could contribute to confirm RO as an ore concentration mechanism (Japas et al., 2015 and reference therein).

7. Conclusions

During San Pedro porphyry copper deposit formation, significant changes in physico-chemical and stress conditions occurred, favoring RO activation during D-vein formation. These changes explain the differences between D₁- and D₂-vein ore paragenesis considering the RO mechanism.

The presence of a phyllic membrane, and pressure and temperature conditions during *La Salvadora* D₂-vein formation allowed RO to activate, resulting in low osmotic differentiation of Cu, Zn, Ag and Pb and leading to ore paragenesis atypical for a porphyry copper deposit. Furthermore, under the temperature conditions at which RO takes place (325°-175 °C) hydrothermal sealing can occur resulting in hydrothermal fluid overpressure, necessary to activate RO.

Besides pressure and temperature, other physico-chemical parameters constraining RO filtration include pH and Eh conditions; the former affecting the rate of retention, the latter modifying the osmotic behavior of Zn (COD) and defining therefore the Zn alternative affinity to Cu^{2+} or

to Pb/Ag

Correlation between metal distribution/concentration and the effectiveness of the membrane in constraining osmotic differentiation (mainly controlled by temperature) indicates RO as a feasible natural mechanism for metal concentration at the phyllic alteration sub-stage in the San Pedro porphyry copper deposit, allowing to consider RO as a feasible metal concentration mechanism to be extrapolated to other porphyry-type deposits.

Declaration of Competing Interest

The authors declare that they have no known competing financial interests or personal relationships that could have appeared to influence the work reported in this paper.

Appendix A. Supplementary data

Supplementary data to this article can be found online at https://doi.org/10.1016/j.oregeorev.2022.104746.

References

Abhang, R.M., Wanib, K.S., Patilc, V.S., Pangarkara, B.L., Parjanea, S.B., 2013. Nanofiltration for recovery of heavy metal ions from waste water - a review. Int. J. Res. Environ. Sci. Technol. 3, 29–34.

Agboola, O., Maree, J., Kolesnikov, A., Mbaya, R., Sadiku, R., 2015. Theoretical performance of nanofiltration membranes for wastewater treatment. Environ. Chem. Lett. 13 (1), 37–47. https://doi.org/10.1007/s10311-014-0486-y.

Al-Alawy, A.F., Salih, M.H., 2017. Comparative study between nanofiltration and reverse osmosis membranes for the removal of heavy metals from electroplating wastewater. J. Eng. 23, 1–21.

Al-Mutaz, I.S., Al-Ghunaimi, M.A., 2001. Performance of reverse osmosis units at high temperatures. IDA World Congr. Desalination and Water Reuse Proc, Bahrain, pp. 1–9.

Amjad, A., Zibrida, J.F., Zuhl, R.W., 1998. Reverse osmosis technology, fundamentals and water applications. Ann. Convention and Exposition, Assoc. Water Technol. Proc. Washington, 1–18.

Anilema-Pilamunga, L.E., Martínez-Ortíz, K.P., 2018. Remoción de colorantes de efluentes de plantas textileras usando arcilla como material adsorbente de bajo costo. Facultad de Ingeniería. Universidad Nacional de Chimborazo 68.

Azaman, F., Nor, M.A.A.M., Abdullah, W.R.W., Razali, M.H., Zulkifli, R.C., Zaini, M.A.A., Ali, A., 2021. Review on natural clay ceramic membrane: Fabrication and application in water and wastewater treatment. Malaysian Journal of Fundamental and Applied Sciences 17, 62–78.

Bartels, C., Franks, R., Rybar, S., Schierach, M., Wilf, M., 2005. The effect of feed ionic strength on salt passage through reverse osmosis membranes. Desalination 184, 185–195.

Becker, G.F., 1892. Quicksilver ore deposits. In: Day, D.D. (Ed.), Mineral Resources of the United States for 1892. U.S. Geol, Survey Report, pp. 139–168.

Berry, F.A.F., 1969. Relative factors influencing membrane filtration effects in geologic environments. Chem. Geol. 4, 295–301.

Camarillo-Blas, R. 2005. Separación selectiva de metales pesados en efluentes industriales mediante tecnología PSU. Ph.D. Thesis, Universidad de Castilla - La Mancha, 317p.

Cathelineau, M., 1988. Cation site occupancy in chlorites and illites as a function of temperature. Clays Clay Miner. 23 (4), 471–485.

Chianese, A., Ranauro, R., Verdone, N., 1999. Treatment of landfill leachate by reverse osmosis. Water Res. 33 (3), 647–652.

Childress, A., Elimelech, M., 2000. Relating nanofiltration membrane performance to membrane charge (Electrokinetic) characteristics. Environ. Sci. Technol. 34, 3710–3716.

Cingolani, C.A. 2017. Pre-Carboniferous evolution of the San Rafael Block, Argentina. Implications in the SW Gondwana margin: An introduction. In: Cingolani, C.A. (Ed.)

Pre-Carboniferous evolution of the San Rafael Block, Argentina, Springer Earth System Sciences. doi: 10.1007/978-3-319-50153-6_1.

Cooke, D.R., Hollings, P., Walshe, J.L., 2005. Giant porphyry deposits - Characteristics, distribution, and tectonic controls. Econ. Geol. 100, 801–818.

Corbett, G.J., and Leach, T. 1997. Southwest Pacific rim gold-copper systems: Structure, alteration and mineralization, Short course manual. 318 pp.

Cosgrove, J.W. 1995. The expression of hydraulic fracturing in rocks and sediments. In Amee, M.S. (Ed.) Fractography: fracture topography as a tool in fracture mechanics and stress analysis. Geol. Soc. Lond. Spec. Publ. 92, 187-196. https://doi.org/10.1144/GSL.SP.1995.092.01.10.

Cox, S.F., 2010. The application of failure mode diagrams for exploring the roles of fluid pressure and stress states in controlling styles of fracture-controlled permeability enhancement in faults and shear zones. Geofluids 10, 217–233. https://doi.org/10.1111/j.1468-8123.2010.00281.x.

Cristiano, E., Hu, Y.-J., Siegfried, M., Kaplan, D., Nitsche, H., 2011. A comparison of Point of Zero Charge measurement methodology. Clays Clay Miner. 2, 107–115.

Davicino, R., 2008. A review of the Anchoris project, Mendoza. Argentina. Internal Report 1–39.

De Sitter, L.U., 1947. Diagenesis of oil-field brines. Amer. Assoc. Petrol. Geol. Bull. 31, 2030–2040.

Deyell, C.L., 2005. Sulfur isotope zonation at the Mt Polley alkalic porphyry Cu–Au deposit, British Columbia, Canada. In: Mao, J., Bierlein, F.P. (Eds.), Mineral Deposit Research: Meeting the Global Challenge. Springer Berlin Heidelberg, Berlin, Heidelberg, pp. 373–376. https://doi.org/10.1007/3-540-27946-6_98.

Dilles, J.H., John, D.A., 2020. Porphyry and epithermal mineral deposits. Encyclopedia of Geology, 30p. https://doi.org/10.1016/B978-0-08-102908-4.00005-9.

Donnan, F.G., 1995. Theory of membrane equilibria and membrane potentials in the presence of no-dialyzing electrolytes. A contribution to physical-chemical physiology. Membr. Sci. 100, 45–55.

Dupont, 2021. Nanofiltration (NF) – using pressure-driven separation for high rejection of multivalent ions. www.dupont.com. Accessed January 2021.

Emalsa, 2007. Curso de Osmosis Inversa. htp://www.emalsa.es/3/3_10_7.php.

Filmtec, 2012. FILMTEC™ membranes. http://www.filmtec.com.

Franks, R., Bartels, C., Nagghappan, L.N.S.P., 2009. Performance of a reverse osmosis system when reclaiming high pH - high Temperature wastewater. AWWA Membr. Technol. Conf, Memphis, TN.

Freeman, S.D.N., Majerle, R.J., 1995. Silica fouling revisited. Desalination 103, 113–115.

Fritz, S.J., Whitworth, T.M., 1994. Hyperfiltration-induced fractionation of lithium isotopes: ramifications relating to representativeness of aquifer sampling. Water Resources Research 30, 225–235.

Fritz, S.J., Hinz, D.W., Grossman, E.L., 1987. Hyperfiltration-induced fractionation of carbon isotopes. Geochimica et Cosmochimica Acta 51, 1121–1134.

Fritzmann, C., Löwenberg, J., Wintgens, T., Melin, T., 2007. State-of-the-art of reverse osmosis desalination. Desalination 216, 1–76.

Ghiu, S.M.S., 2003. Mass transfer of ionic species in direct and reverse osmosis processes. Graduate School Theses and Dissertations. In: University of Florida, p. 188 pp.

Giwa, A., Ogunribido, A., 2012. The applications of membrana operations in the textile industry: a review. Br. J. Appl. Sci. Technol. 2, 296–310.

Gómez, A.L.R., 2013. Caracterización metalogenética del distrito minero San Pedro y su vinculación con el magmatismo gondwánico, Bloque de San Rafael, Mendoza. Ph.D. Thesis, Universidad de Buenos Aires 327 pp.

Gómez, A.L.R., Rubinstein, N., Valencia, V.A., 2015. Gondwanan magmatism with adakite-like signature linked to Cu (Mo)-porphyry deposits from the San Rafael Massif, Mendoza province. Argentina. Chem. Erde. 75 (1), 89–104.

Gómez, A.L.R., Ulrich, Th., Rubinstein, N.A., 2021. The magmatic-hydrothermal evolution of the San Pedro Porphyry Cu-(Mo) deposit: implications for the metallogenesis of the Permian magmatism in the western margin of Gondwana. Resour. Geol. 71 (2), 93–104. https://doi.org/10.1111/rge.v71.210.1111/rge.12251.

Gustafson, L.B., Hunt, J.P., 1975. The porphyry copper deposit at El Salvador Chile. Econ. Geol. 70, 857–912.

Gustafson, L.B., Quiroga, J., 1995. Patterns of mineralization and alteration below the porphyry copper orebody at El Salvador. Chile. Econ. Geol. 90, 2–16.

Hagmeyer, G., Gimbel, R., 1998. Modelling the salt rejection of nanofiltration membranes for ternary ion mixtures and for single salts at different pH values. Desalination. 117, 247–256.

Hart, M.L., 2013. Low head hyperfiltration through intact Burlington Limestone and Jefferson City Dolomite discs. Applied Geochemistry 33, 357–365.

Hawlader, M.N.A., Ho, J.C., Chua, K.T., 2000. Desalination of seawater: an experiment with RO membranes. Desalination 132, 275–280.

Hedenquist, J.W., Richards, J., 1998. The influence of geochemical techniques on the development of genetic models for porphyry copper deposits. In: Richards, J.P., Larson, P.B. (Eds.), Rev. Econ. Geol. 10, 235–256.

Japas, M.S., Kleiman, L.E., 2004. El Ciclo Choiyoi en el Bloque de San Rafael: de la orogénesis tardía a la relajación mecánica. Asoc. Geol. Argent. Serie D: Publ. Espec. 7, 89–100.

Japas, M.S., Rubinstein, N.A., Kleiman, L.E., 2013. Strain fabric analysis applied to hydrothermal ore deposits emplaced during changing geodynamical conditions (Infiernillo and Las Picazas, San Rafael Massif, Argentina). Ore Geol. Rev. 53, 357–372.

Japas, M.S., Rubinstein, N.A., Gómez, A.L.R., 2015. Reverse Osmosis contributing to metal zoning in porphyry type deposits, a case study. Ore Geol. Rev. 71, 191–202.

Japas, M.S., Oriolo, S., Samuel, V., 2019. Coupling between fluids and rock deformation in the continental crust: Preface. Geosci. Front. 10 (6), 2085–2092. https://doi.org/10.1016/j.gsf.2019.07.001.

Japas, M.S., Gómez, A.L.R., Rubinstein, N.A., 2021. Unravelling the hydro-mechanical evolution of a porphyry-type deposit by using vein structures. Ore Geol. Rev. 133, 104074. https://doi.org/10.1016/j.oregeorev.2021.104074.

Jarusutthirak, Ch., Mattaraj, S., Jiraratananon, R., 2007. Influence of inorganic scalants and natural organic matter on nanofiltration membrane fouling. J. Membr. Sci. 287, 138–145.

Kharaka, Y.K., Berry, F.A., 1973. Simultaneous flow of water and solutes through geologic membranes. I. Experimental investigation. Geochim. Cosmochim. Acta 37, 2577–2603.

Kleiman, L.E., Japas, M.S., 2009. The Choiyoi volcanic province at 34–36°S (San Rafael, Mendoza, Argentina): implications for the late Palaeozoic evolution of the southwestern margin of Gondwana. Tectonophysics 473, 283–299. https://doi.org/10.1016/j.tecto.2009.02.046.

Korzeniewski, L., Rubinstein, N., Gómez, A., 2012. Condiciones físico-químicas de los fluidos mineralizantes en el pórfiro de Cu San Pedro, Mendoza (Argentina). Rev. Asoc. Geol. Argent. 69, 13–18.

Kouzmanov, K., Pokrovski, G.S., 2012. Chapter 22: Hydrothermal Controls on Metal Distribution in Porphyry Cu (-Mo-Au) Systems. Soc. Econ. Geol., Spec. Publ. 16, 573–618.

Landtwing, M.R., Pettke, T., Halter, W.E., Heinrich, C.A., Redmond, P.B., Einaudi, M.T., Kunze, K., 2005. Copper deposition during quartz dissolution by cooling magmatic-hydrothermal fluids: The Bingham porphyry. Earth Planet. Sci. Lett. 235, 229–243.

Lanxess, 2013. Reverse Osmosis, Theory, Principles of reverse osmosis membrane separation. 01_lewabrane_manual_ro_theory_01.pdf. http://lewabrane.com/.

Lastra, A., Gómez, D., Romero, J., Francisco, J.L., Luque, S., Álvarez, J.R., 2004. Removal of metal complexes by nanofiltration in a TCF pulp mill, technical and economic feasibility. J. Membr. Sci. 242, 97–105.

Lepeltier, C., 1969. A simplified statistical treatment of geochemical data by graphical representation. Econ. Geol. 64, 538–550.

Li, D., Yan, Y., Wang, H., 2016. Recent advances in polymer and polymer composite membranes for reverse and forward osmosis processes. Progress in Polymer Science 61, 104–155. https://doi.org/10.1016/j.progpolymsci.2016.03.003.

Liu, S.X., 2007. Food and Agricultural Wastewater Utilization and Treatment. Blackwell Publishing.

Llambías, E.J., Kleiman, L.E., Salvarredi, J.A., 1993. Magmatismo gondwánico de Mendoza. Relat. 13° Congr. Geol.. Argent. 53–64.

Llorente-Ayza, M.M., 2017. Membranas cerámicas de bajo coste para el tratamiento de aguas residuales. PhD Thesis, Universitat Jaume I de Castelló 300 p.

Lowell, J.D., Gilbert, J.M., 1970. Lateral and vertical alteration mineralization zoning in porphyry ore deposits. Econ. Geol. 65, 373–408.

Lueth, V.W., Whitworth, T.M., 2009. A hyperfiltration model for copper mineralization at the Abo Mine, Scholle District, New Mexico. N. M. Geol. Soc. Guideb. 60, 102–104.

MacKay, R.A., 1946. The control of impounding structures on ore deposition. Econ. Geol. 41, 13–46.

Maffini, M.N., Wemmer, K., Radice, S., Oriolo, S., D'Eramo, F., Coniglio, J., Demartis, M., Pinotti, L., 2017. Polymetallic (Pb-Zn-Cu-Ag±Au) vein-type deposits in brittle-ductile transtensional shear zones, Eastern Sierras Pampeanas (Argentina): age constraints and significance for the Late Paleozoic tectonic evolution and metallogenesis. Ore Geol. Rev. https://doi.org/10.1016/j.oregeorev.2017.07.003.

Magara, K., 1974. Compaction, ion filtration, and osmosis in shale and their significance in primary migration. Am. Assoc. Petrol. Geol. Bull. 58, 283–290.

Mänttäri, M., Pihlajamäki, A., Nyström, M., 2006. Effect of pH on hydrophilicity and charge and their effect on the filtration efficiency of NF membranes at different pH. J. Membr. Sci. 280, 311–320.

Mei, Y., Sherman, D.M., Liu, W., Brugger, J., 2013. *Ab initio* molecular dynamics simulation and free energy exploration of copper(I) complexation by chloride and bisulfide in hydrothermal fluids. Geochim. Cosmochim. Acta 102, 45–64.

Mei, Y., Liu, W., Sherman, D.M., Brugger, J., 2014. Metal complexation and ion hydration in low density hydrothermal fluids: *Ab initio* molecular dynamics simulation of Cu(I) and Au(I) in chloride solutions (25–1000°C, 1–5000 bar). Geochim. Cosmochim. Acta 131, 196–212.

Mei, Y., Sherman, D.M., Liu, W., Etschmann, B., Testemale, D., Brugger, J., 2015. Zinc complexation in chloride-rich hydrothermal fluids (25–600°C): A thermodynamic model derived from *ab initio* molecular dynamics. Geochim. Cosmochim. Acta 150, 265–284.

Microdyn-Nadir, 2019. Membrane filtration processes, Dead-end vs. Cross flow. Technical Bulletin, TB-025. https://www.microdyn-nadir.com. Accessed January 2021.

Murthy, Z.V.P., Chaudhari, L.B., 2009. Separation of binary heavy metals from aqueous solutions by nanofiltration and characterization of the membrane using Spiegler-Kedem model. Chem. Eng. J. 150, 181–187.

Ong, S.L., Zhou, W., Song, L., Ng, W.J., 2002. Evaluation of feed concentration effects on salt / ion transport through RO / NF membranes with the Ernst-Planck-Donnan model. Environ. Eng. Sci 19, 429–439.

Ozaki, H., Sharma, K., Saktaywin, W., 2002. Performance of an ultra-low-pressure reverse osmosis membrane (ULPROM) for separating heavy metal: effects of interference parameters. Desalination 144 (1–3), 287–294.

Pal, P. 2015. Groundwater arsenic remediation. Treatment Technology and scale UP. Elsevier. doi: 10.1016/C2013-0-19489-5.

Palacio-Martínez, L., 1998. Caracterización estructural y superficial de membranas microporosas. PhD Thesis. Universidad de Valladolid, p. 336 p.

Peacock, D.C.P., Anderson, M.W., Rotevatn, A., Sanderson, D.J., Tavarnelli, E., 2017. The interdisciplinary use of "overpressure". J. Volcanol. Geotherm. Res. 341, 1–5. https://doi.org/10.1016/j.jvolgeores.2017.05.005.

Pirajno, F., 2009. In: Hydrothermal Processes and Mineral Systems. Springer Netherlands, Dordrecht.

Qin, J.-J., Oo, M.H., Coniglio, B., 2005. Relationship between feed pH and permeate pH in reverse osmosis with town water as feed. Desalination 177, 267–272.

Rautenbach, R., Linn, Th., 1996. High-pressure reverse osmosis and nanofiltration, a "zero discharge" process combination for the treatment of waste water with severe fouling/scaling potential. Desalination 105, 63–70. https://doi.org/10.1016/0011-9164(96)00059-9.

Reed, M.H., Palandri, J., 2006. Sulfide mineral precipitation from hydrothermal fluids. Rev. Mineral. Geochem. 61, 609–631.

Rocha-Campos, A.C., Basei, M.A., Nutman, A.P., Kleiman, Laura E., Varela, R., Llambías, E., Canile, F.M., da Rosa, O. de C.R., 2011. 30 million years of Permian volcanism recorded in the Choiyoi igneous province (W Argentina) and their source for younger ash fall deposits in the Paraná Basin: SHRIMP U-Pb zircon geochronology evidence. Gondwana Res. 19 (2), 509–523.

Rogel-Hernández, E., Espinoza-Gómez, H., Lin, S.W., Ames, A., García, C., Ramos, R., 2006. Remoción de Ca2+, Fe2+, Pb2+, empleando una electrocelda de membranas de ultrafiltración. 5° Congr. Internac. y 11° Congr Nac. Cs. Ambient. http://www 2006 uaemex.mx/Red_Ambientales/docs/memorias/Extenso/TA/EC/TAC-47.pdf).

Rosenberg, P.E., 2002. The nature, formation, and stability of end-member illite: a hypothesis. Am. Mineral. 87 (1), 103–107.

Rubinstein, N., Bevins, R.E., 2004. Mineralization of La Salvadora deposit, Province of Mendoza. Argentina. N. Jahrb. Mineral. Mon. 6, 241–252.

Rusk, B.G., Reed, M.H., Dilles, J.H., 2008. Fluid inclusion evidence for magmatic-hydrothermal fluid evolution in the porphyry copper-molybdenum deposit at Butte. Montana. Econ. Geol. 103, 307–334.

Sato, M., 1992. Persistency field Eh-pH diagrams for sulfides and their application to supergene oxidation and enrichment of sulfide ore bodies. Geochim. Cosmochim. Acta 56, 3133–3156.

Schäfer, A.I., Fane, A.G., Waite, T.D., 2002. Nanofiltration – principles and application. Elsevier.

Schirg, P.G., 2001. Introducción a la teoría y práctica de la técnica de membranas. GmbH Report. www.membran.com.

Seedorff, E., Dilles, J.H., Proffett Jr., J.M., Enaudi, M.T., Zurcher, L., Stavast, W.J.A., Johnson, D.A., Barton, M.D., 2005. Porphyry deposits, Characteristics and origin of hypogene features. Econ. Geol. 100th Anniv. Vol, 251–298.

Seeward, T.M., Williams-Jones, A.E., Migdisov, A., 2013. The chemistry of metal transport and deposition by ore-forming hydrothermal fluids. In: Holland, H., Turekian, K. (Eds.), Treatise of Geochemistry, Geochemistry of mineral deposits, Chapter 13, 29–57. https://doi.org/10.1016/B978-0-08-095975-7.01102-5.

Sibson, R.H., 1998. Brittle failure mode plots for compresional and extensional tectonic regimes. J. Struct. Geol. 20, 655–660.

Sibson, R.H., 2000. A brittle failure mode plot defining conditions for high-flux flow. Econ. Geol. 95, 41–48.

Sillitoe, R.H., 2010. Porphyry copper systems. Econ. Geol. 105, 3–41.

Smith, R.M., Martell, A.E., 1976. Critical stability constants. Volume 4: Inorganic complexes. Springer Science+Business Media, New York, pp. 255–pp.

Spirakis, Ch., 1977. The role of semipermeable membranes in the formation of certain Vanadium-Uranium deposits. Econ. Geol. 72, 1442–1448.

Sposito, G., 1989. The chemistry of soils. Oxford University Press, p. 277 p.

Szoke, S., Patzay, G., Weiser, L., 2002. Characteristics of thin-film nanofiltration membranes at various pH-values. Desalination 151, 123–129.

Tanninen, J., Nyström, M., 2002. Separation of ions in acidic conditions using NF. Desalination 147, 295–299.

Tosdal, R.M., Dilles, J.H, 2020. Creation of permeability in the porphyry Cu environment. In: Rowland, J., Rhys, D. (Eds.), Rev. Econ. Geol. 21, 173–204. https://doi.org/10.5382/rev.21.05.

Tosdal, R.M., Richards, J.P. 2001. Magmatic and structural controls on the development of porphyry Cu ± Mo ± Au deposits. In: Richards, J.P., Tosdal, R.M., eds., Structural controls on ore deposits. Rev. Econ. Geol. 14, 157-181.

Ulrich, Th., Heinrich, C.A., 2001. Geology and alteration geochemistry of the porphyry Cu-Au deposit at Bajo de la Alumbrera. Argentina. Econ. Geol. 96, 1719–1742.

Van der Bruggen, B. 2018. Microfiltration, ultrafiltration, nanofiltration, reverse osmosis and forward osmosis. In: Luis, P. (ed.), Fundamental modeling of membrane systems. Chapter 2, 25-70. doi: 10.1016/B978-0-12-813483-2.00002-2.

Villaluenga, J.P.G., Seoane, B., Barragán, V.M., Ruiz-Bauzá, C., 2006. Thermo-osmosis of mixtures of water and methanol through a Nafion membrane. J. Membr. Sci. 274 (1–2), 116–122.

Whitworth, T.M., 1993. Hyperfiltration-induced isotopic fractionation: mechanisms and role in the subsurface. PhD. Dissertation,. Purdue University, p. 222 p..

Whitworth, T.M., 1998. Clay membranas. In: Marshall, C.P., Fairbridge, R.W. (Eds.), Encyclopedia of Geochemistry. Kluwer Academic Publishers, pp. 83–85.

Whitworth, T.M., Haneberg, W.C., Mozley, P.S., Goodwin, L.B., 1999. Solute-sieving-induced calcite precipitation on pulverized quartz sand: Experimental results and implications for the membrane behavior of fault gouge. Geophysical Monograph-American Geophysical Union 113, 149–158.